# Design and characterization of a durable and highly efficient energy-harvesting electrochromic window

Eri Amasawa

A thesis submitted in partial fulfillment
of the requirements for the degree of

Master of Science in Engineering

University of Washington

2013

Committee:

Dr. Minoru Taya
Dr. Joyce Cooper
Dr. Christine Luscombe
Dr. Yasuo Kuga

Program Authorized to Offer Degree: Mechanical Engineering

©Copyright 2013

Eri Amasawa

University of Washington

## Abstract

Design and characterization of a durable and highly efficient energy-harvesting electrochromic window

Eri Amasawa

Chair of the Supervisory Committee:
Professor Minoru Taya
Department of Mechanical Engineering

With the growing global energy demands, electrochromic window (ECW) technology has attracted great attention for its ability to reversibly change the transmittance of incoming light through applied moderate potential. While ECW has a great potential to conserve energy from lighting and air conditioning in buildings, ECW still consumes energy; ECW should be self-powered for further energy conservation. In this study, a new design of energy-harvesting electrochromic window (EH-ECW) based on fusion of two technologies, organic electrochromic window and dye-sensitized solar cell (DSSC) is presented. Unlike other self-powered smart windows such as photoelectrochromic device that only contains two states (i.e. closed circuit colored state and open circuit bleaching state), EH-ECW allows active tuning of transmittance through varying applied potential and function as a photovoltaic cell based on DSSC. The resulting device demonstrates fast switching rate of 1 second in both bleaching and coloring process through the use of electrochromic polymer as a counter electrode layer. In order to increase the transmittance of the device, cobalt redox couple and light colored yet efficient organic dye are employed. The organic dye utilized contains polymeric structure, which

contributes to high cyclic stability. The device exhibits power conversion efficiency (PCE) of 4.5 % under AM 1.5 irradiation (100 mW/cm$^2$), change in transmittance ($\Delta T = T_{max} - T_{min}$) of 34 % upon applied potential, and shows only 3 % degradation in PCE after 5000 cycles.

## Table of Contents

## List of Figures

## List of Tables



## List of Schemes

## Acknowledgements

This research was supported by a grant from National Science Foundation to the University of Washington (NSF EFRI 1038165), where I would like to express gratitude for discussions with our collaborators, Dr. Christine Luscombe, Department of Materials Science and Engineering, University of Washington, and Dr. Yasuo Kuga, Department of Electrical Engineering, University of Washington. Additionally, this work was completed through collaboration with Shinshu University, supported by Grants-in-Aid for Scientific Research (B) (No. 22350086) from Japan Society for the Promotion of Science (JSPS). I would like to express special gratitude for Dr. Mutsumi Kimura for fruitful discussions, vast generosity, and invaluable experience at his laboratory. Last but not least, I would like to acknowledge Dr. Minoru Taya, Naoki Sasagawa, Risa Wampler, colleagues at the University of Washington Center for Intelligent Materials and Systems and students from Kimura Lab at Shinshu University who assisted me through my master's research.

# Chapter 1: Introduction to Electrochromic Window

## 1.1 Background

The United States consumes nearly as much primary energy as China in 2010 and 41 % of that is consumed in building sector.[1] When the contents of energy consumption in building sector are analyzed, it was found that about 55 % is consumed in heating, cooling, and lighting (**Figure 1**). In discussions of energy conservation in buildings, it was found that windows play a big role in the temperature and the brightness of the indoor environment. An example of heat flow is described in **Figure 2**. Depending on the window quality in use, indoor environment experiences great amount of heat gain during summer time. The power loss from the conduction through windows or walls can be expressed by **Equation 1**, where U-value is the thermal transmittance of a material. [2] More insulating the wall or windows (e.g. thicker) are, smaller the U-value becomes. In order to dynamically control the U-value for energy conservation, electrochromic windows (ECW) have attracted much of the attention in recent years.

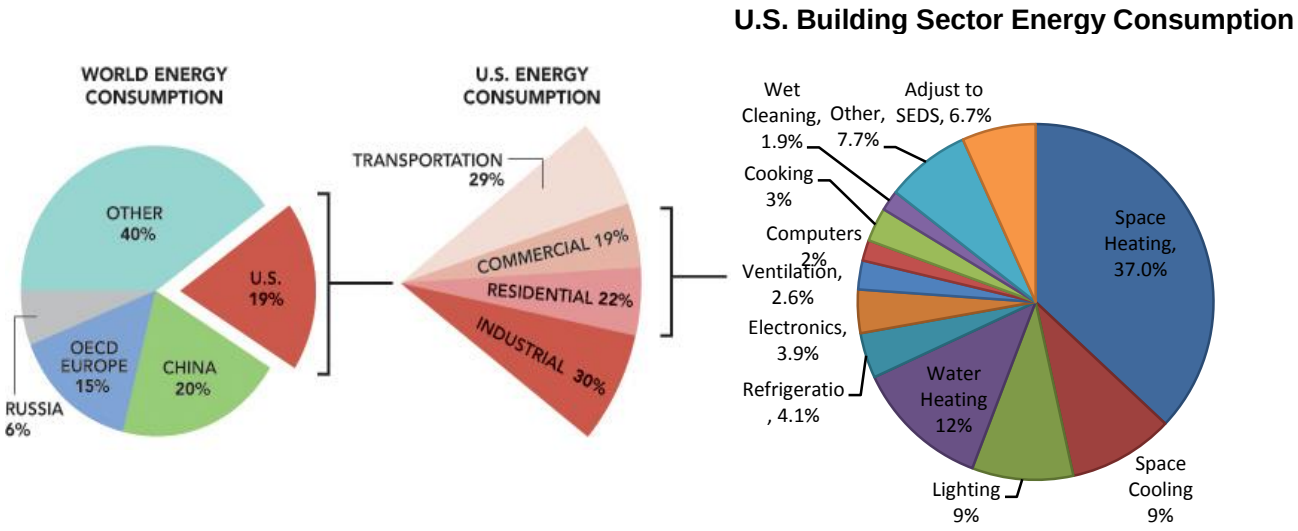


Figure 1: U.S. energy consumption and its breakdown in building sector [1]

$$Power\ loss = area \times U \times temperature\ difference \quad \text{(Equation 1)}^{2}$$

ECW is a thin film device that can reversibly change its optical properties upon applied potential, which of the mechanism is based on oxidation and reduction of an electrochromic film. ECW is considered as an emerging alternative smart window technology that can be utilized on windows of not only buildings, but also automobiles and aircrafts. Through reversibly changing the transmittance, reflectance, absorbance, and emittance of the incoming irradiation through window, [3] energy savings from cooling and heating are anticipated, as the heat gain and heat loss through the windows can be substantial in buildings. Compared to other smart window technology (i.e. suspended particle display and liquid crystal display), ECW has advantages such as color memory, high contrast ratio, broad color availability, long lifetime, and ability to adjust the transmittance through varying applied potentials.[4]

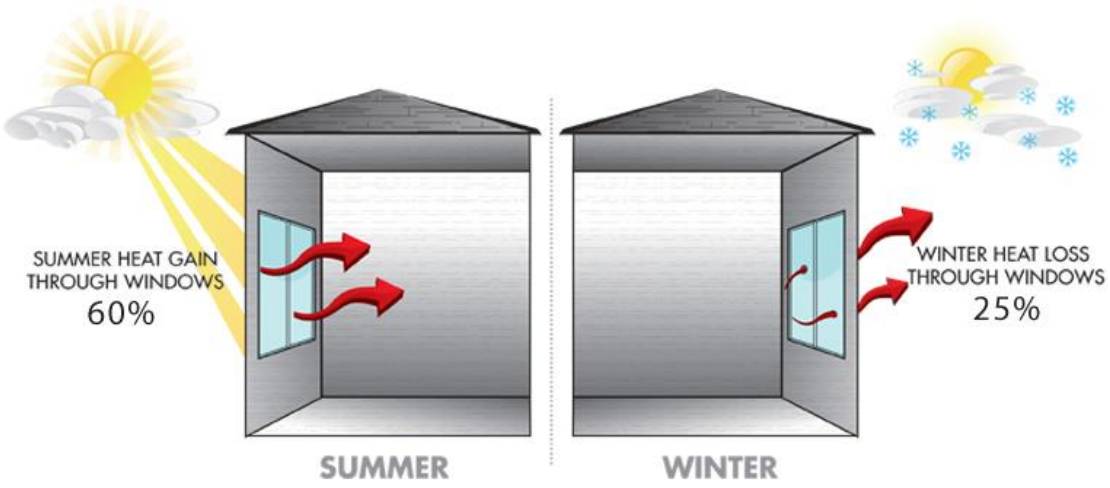


Figure 2: Schematic of heat energy flow to/from outdoor environment to indoor environment [5]

## 1.2 Device components and mechanisms

The electrochromic device generally consists of multilayers, where the basis is a glass or plastic covered by a transparent conductive film (i.e. most commonly indium-tin oxide (ITO), fluorine-

doped tin oxide (FTO), and antimony-doped tin oxide (ATO)) on which one or multiple cathodic electrochromic layer(s) are affixed (**Figure 3**). These are followed by a layer of ion conductor, followed by an ion-storage film or one or multiple complimentary anodic electrochromic layers and another transparent conducting film. Upon applied potential, ions are intercalated or extracted from the electrochromic layer, switching their optical properties between their oxidized and reduced form. The ions should be small for high mobility and ability to be intercalated, where the common ions are lithium ions ($Li^+$) and protons ($H^+$).[3] Most favorable electrochromics are those that are reflecting in their colored state instead of absorbing, but this has been found very difficult and thus most electrochromics are absorbing.[6] By combining different type of electrochromics, ion-storage films and ion conductors, different properties can be obtained for the device, where the modulation range, durability and switching speeds can be optimized.

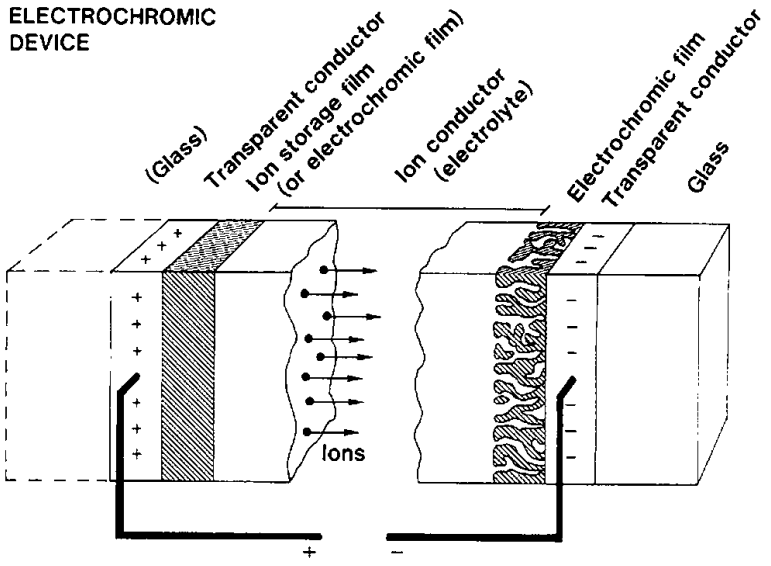


Figure 3: Basic design of an electrochromic device, indicating transport of positive ions under the action of an electric field[3]

The electrochromic (EC) materials utilized for ECW today can be largely divided into three groups: transition metal oxides, organic or organometallic small molecules, and conductive

polymers (i.e. polyaniline, poly(3,4-ethylenedioxythiophene) (PEDOT), and poly(3,4-propylenedioxythiophene) (PProDOT)). ECW device based on transition mental oxides such as $WO_3$, NiO, and $Nb_2O_5$ exhibits excellent long-term durability and high transmittance difference ($\Delta T = T_{max} - T_{min}$), which has helped endeavor the ECW technology to become commercially available.[3] However, ECW device based on such inorganic materials suffers from slow switching speed and high cost of manufacturing due to the high temperature processing. The shortcoming of inorganic materials also adds to the cost of materials. In a search of inorganic substituents, conductive organic materials have been growing interests. Although organic or organometallic small molecules with electrochromic property, such as Prussian blue, viologen [4,7] and phthalocyanines[6] have been researched extensively, there are numerous disadvantages of small molecules, such as film fracture, loss of adhesion and short lifetime. On the other hand, conductive polymers have advantages over inorganic materials such as low cost and ease of processing. There is a high degree of color tailorability by fine turning of the energy gap and much higher coloration efficiency. The well-known electrochromic conductive polymers include most aromatic organic molecules, such as polypyrrole, polythiophene, and polyaniline. However, all electroactive polymers are potentially electrochromic, which makes this subclass a progressive research field. The ECW device based on electroactive polymers have proven advantages of low power consumption (i.e. power is only required intermittently during switching), moderate switching voltages (1-5 V), low polarization, long optical memory, and ease of processing at large scale. In this study, electroactive layer based on organic electronic material is utilized; thus, the discussions on the mechanism of electrochromism will be focused on those in organic polymers.

## 1.3 Mechanism of electrochromism in organic electronic polymers

In this section, mechanism of electrochromism in organic electronic polymers will be discussed. Although the discussion places a focus on conjugated polymers, it is well to note that these concepts are applicable to small molecules as well.

### 1.3.1 Conjugated polymer

Today, people carry around portable electronics that incorporate semiconducting polymers without a realization. The cell phones and television screens that incorporate organic light emitting diodes (OLEDs), field effect transistors (FETs) are already available in the market. These electronic polymers share the same π-conjugated structure. By definition, conjugated molecules are those composed of alternating single and double or triple bonds, and conjugated polymers are the polymer with conjugated repeat units or structure.[8] However, the conjugation does not inherently provide conductive properties, but the doping process creates conjugated polymers to increase conductivity substantially. Conventionally, polymers are insulator by nature, with the typical intrinsic conductivity of about $10^{-12}$ to $10^{-6}$ S/cm, due to the small concentration of charge carriers and their low mobility. In 1977, doping phenomena of conducting polymers was discovered, which showed the 13 orders of magnitude increase in the DC conductivity of polyacetylene.[9]

### 1.3.2 Doping phenomena in conjugated polymers

Doping in polymer science is essentially an oxidation or reduction process. Depending on how easily the conjugated polymer becomes oxidized or reduced, polymers can be identified as “p-type” or “n-type”, respectively. The property of the material that differentiates one from the other is all relative to the electronic structure of one another and the work function of the metals being dealt with in a device. To better understand the idea, it is well to approach from the role of

conjugated polymers in an optoelectronic device, such as OLEDs. **Figure 4** illustrates the charge carrier movements within OLED, which defines the two types of semiconductors: p-type semiconductor refers to a semiconducting material which of its majority of charge carriers is holes, whereas the majority of charge carriers are electrons in n-type semiconductors.[10]

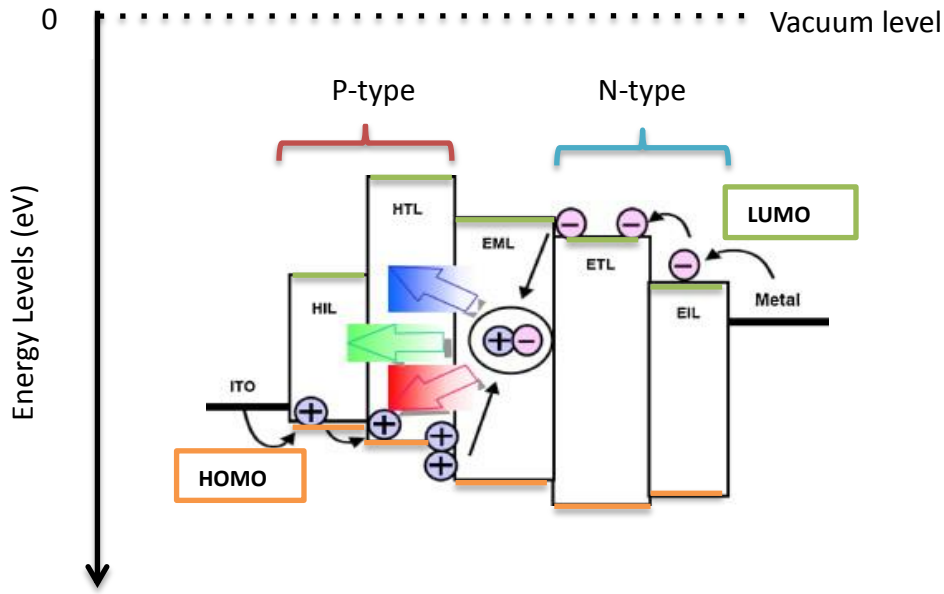


Figure 4: Energy diagram of a typical OLED. The acronyms are: Hole injection layer (HIL), hole transporting layer (HTL), emission layer (EML), electron transporting layer (ETL), and electron injection layer (EIL). Figure was modified from the original image by the author [11]

In order for electrons to travel from one material to another (e.g. electron injection from metal to EIL), the Lowest Unoccupied Molecular Orbital (LUMO) of the organic semiconductors must be at least 0.3 eV lower than the work function of the cathode metal for charge transfer to occur (note that y-axis is reversed because our discussion is based on electron volt), but higher than the LUMO level of EML material for electroluminescence to occur. Subsequently, holes travel though the Highest Occupied Molecular Orbital (HOMO) of the organic semiconductors, which has to be higher than the work function of conductive electrode substrate such as ITO but lower than the HOMO level of EML material. As long as these criteria are met, organic

semiconductors can be categorized into p-type or n-type material in a device. In another word, depending on the material used for electrodes, some organic semiconductors may be used for p-type for one device but n-type for another material combination of a device.

While the definition may seem to allow a wide selection and combination of materials for electronic devices, a common feature of most organic semiconductors is that electron and hole transport is highly unbalanced. This consequence does not mean that the charge mobility is inherently lower for electrons compared with holes; indeed, theoretical studies show that they are at least similar for many organic semiconductors. [12] The reason behind this is due to the presence of extrinsic charge traps that hinder the transport of one type of charge carrier, which are usually associated with oxygen or water impurities. [13] Because of the charge traps, stability in ambient condition is detrimental for the performance of n-type polymers.

With that in mind, there are only small numbers of conjugated polymers that can satisfy the criteria to be n-type. The work function ($\Phi$) of cathodic metals are typically between 3~4 eV (e.g. $\Phi(Al) = 4.3$ eV, $\Phi(Mg) = 3.7$ eV, and $\Phi(Ca) = 2.9$ eV),[8] and the electron affinity level of organic semiconductors are typically in the range of 2~3 eV, which is too small to inject electrons for most electrode metals. Even if low-work function metals, such as calcium or magnesium were to be used, these electrodes themselves are not environmentally stable.[12] On the other hand, HOMO levels of organic semiconductors are generally 4.5~6.5 eV, and the work function of ITO is 4.7~4.8 eV, which provides a variety of options to qualify as p-type materials. Such intrinsic property of conjugated polymers causes the misalignment of the LUMO level with the work function of many metals, and thus contributes to the scarcity of organic materials that can function as n-type materials, compared to p-type materials.

## 1.4 Electrochromism

Most organic molecules and polymers are electrochromic, and they provide infinite possibilities for variety of applications through molecular design. The absorption wavelength of a material is related to the energy bandgap of a material described by **Equation 2**. Since the typical energy gap of organic materials is in the range of 2 ~ 3.5 eV, [8] the color of the organic material falls in the range of visible region as well.

$$\lambda_g\ (nm) = \frac{hc}{E_g(eV)} \qquad \text{(Equation 2)}$$

In the process of electrochromism, upon applied potential, organic molecules or polymers shift its absorption pattern through doping phenomena (i.e. redox reaction). The redox reaction alters the energy levels of the material through introducing radicals, such as polarons and bipolarons. The altered energy levels produce new bandgap, which exhibits different absorption pattern.

In the field of electrochromic polymer, changing the composition of the polymers at the molecular level has been the most extensively investigated approach for color-tuning so far. Indeed, a variety of synthetic strategies have been described over the years spanning varying the overall planarity of the backbones as a function of steric hinderance, changing the electron-rich and –poor character of the building blocks incorporated in the repeat unit, increasing the conjugation lengths via the use of fused heterocycles to reduce the polymers' bond-length alteration, copolymerizing different monomers randomly and in different feed ratios, and so on.[14]

### 1.4.1 Electrochromism of PProDOT-$Me_2$

The neutral color of PProDOT-$Me_2$ is dark blue, and it becomes transmissive light blue upon oxidation. The polarity created by applied potential attracts cation (e.g. $Li^+$) in electrolyte, and the ions become intercalated into the polymeric film of PProDOT-$Me_2$. Cations take away the

electron from the surfur atom in thiophene, resulting in oxidized state (**Figure 5**). The film will remain at oxidized state as long as cations remain intercalated in the film, even without applied potential. This phenomenon is called memory effect in electrochromic materials. The two methane substituents provide high surface area and porous network of PProDOT-$Me_2$ to create good memory effect of the film.

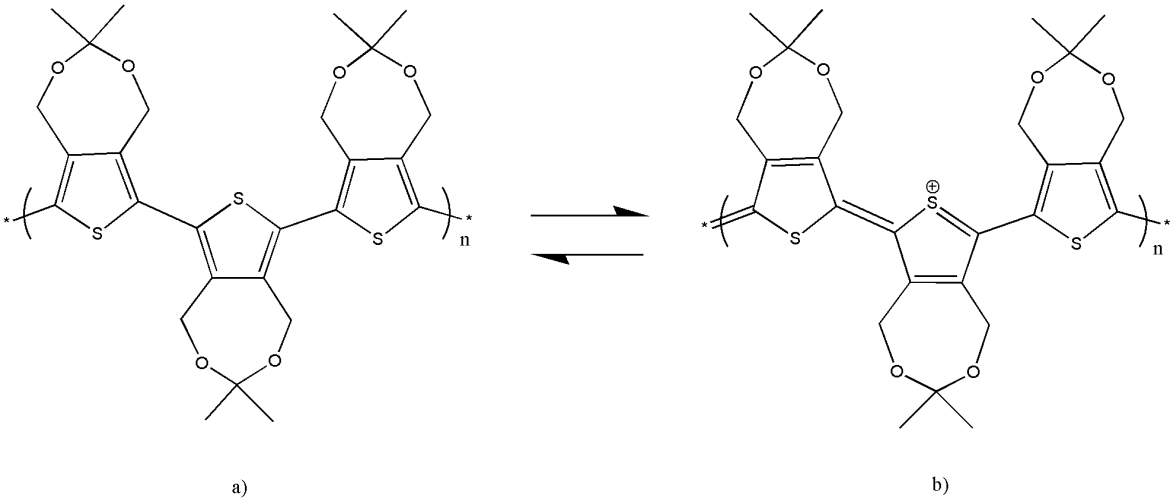


Figure 5: PProDOT-$Me_2$ structure, a) neutral state (colored) and b) oxidized state (bleached)

### 1.4.2 Performance parameters of ECW device

The device performance of ECW is measured through the evaluation of optical and electrochemical properties. Optical properties are evaluated through the transmittance range. Transmittance, *T*, is defined by **Equation 4**, where $P_o$ is the light of radiant power incident on the device and *P* is the radiant power of the transmitted light. [15] Often, transmittance is characterized at various applied potential for ECW, which ultimately provides the maximum transmittance difference described by **Equation 5**.

$$T = \frac{P}{P_o} \qquad \text{(Equation 4)}$$

$$\Delta T = T_{max} - T_{min} \qquad \text{(Equation 5)}$$

$T_{max}$ is the maximum transmittance at bleached state, and $T_{min}$ is the minimum transmittance at colored state, and $\Delta T$ is computed at a specific wavelength. Since ECW is most concerned with the visible range of the incoming irradiation, the wavelength between 300 nm – 800 nm is often investigated. Durability of the optical properties is also evaluated through applying cyclic potentials with fixed time frame, e.g. 5000 cycles of ± 1.5 V with 5 second per step.

The charge capacitance is the measure of electrochemical properties that determines the stability of the electrochromic materials, whether the charge capacitance on both sides of electrodes are balanced. Balanced charge capacitance of working and counter electrode is crucial for long term electrochemical stability of the device.

# Chapter 2: Basics of Dye-Sensitized Solar Cells

## 2.1 Introduction

The sun delivers solar irradiation in the magnitude of terawatts everyday onto the earth's surface. In order to convert the solar energy in a useful form for civilization, there have been tremendous global interests on the research and the development of solar energy harvesting technology for the past half a century. Although Si-based photovoltaic cells has the largest share in the current market, new type of photovoltaic cell has attracted much of the attention for its low fabrication cost and high efficiency in recent years: dye-sensitized solar cells (DSSCs). [16, 17]

## 2.2 Mechanism

DSSC is composed of a transparent conductive glass (generally FTO) with a mesoporous Titanium Oxide ($TiO_2$) nanoparticle layer as a working electrode, dye molecules as a sensitizer to capture photons, electrolyte solution as a mediator, and catalyst coated conductive glass as a counter electrode. **Figure 6** illustrates a schematic of a DSSC with the pathway of electrons shown in arrows.

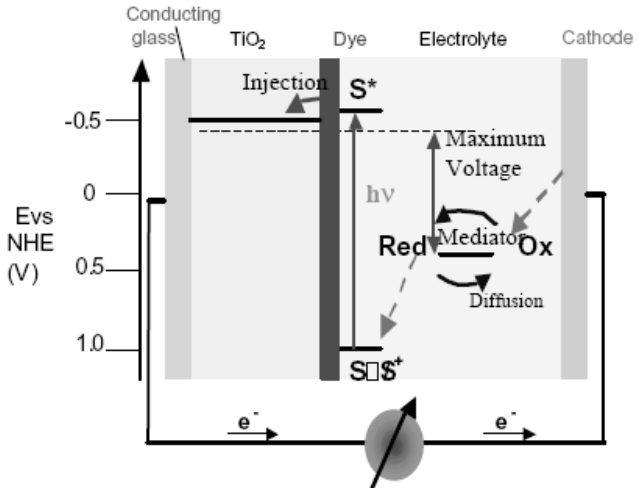


Figure 6: Schematic presentation of the principle of DSSC[18]

In the conventional photovoltaic cells, the semiconductor light harvesting and conduction of the charge carriers under illumination occur in the same material, where a built-in electric field separates photogenerated charge carriers (i.e. electrons and holes) at the interface of semiconductor layer to produce a photocurrent. In contrast, light harvesting is separated from charge carrier transport in DSSCs, which is almost entirely kinetically controlled. [19, 20] Such energy harvesting process is very similar to that of photosynthesis; thus, many researchers refer to the mechanism of DSSC as a biomimetic approach of solar energy conversion. [21]

In DSSC under illumination, photoexcitation by the sensitizer dye molecule leads electron injection into the conduction band of $TiO_2$, followed by the regeneration of oxidized dyes by reducing agent in electrolyte redox couple. The electrons in $TiO_2$ are further transferred toward the conducting glass, and to the external circuit, and ultimately induce electron injection from cathode, which drives the electrochemical redox reaction of electrolyte solution. There is no overall chemical change in the cell; sunlight is simply converted into electrical power. [19] Every component of DSSC contributes to the overall photocurrent efficiency; thus, it is crucial to find the appropriate combination of each material based on its electronic structure, chemical and physical properties.

## 2.3 Performance parameters of DSSC

Commonly, photovoltaic performance of DSSC (or any other solar cells) is evaluated through the measurement of power conversion efficiency ($\eta$, PCE) and incident monochromatic photon-to-electron conversion efficiency (IPCE). The determination of PCE, as shown in **Equation 6** involves short circuit current ($I_{sc}$), open circuit voltage ($V_{oc}$), fill factor, power intensity of irradiation ($P_{in}$), and illuminated cell area ($A_{cell}$). When a DSSC is under illumination with the incident photon flux of $I_{photon}(\lambda)$, the total current flowing in the external circuit ($I_{sc}$) is expressed

as **Equation 7**. Then, IPCE is computed through **Equation 8**, $\eta_{LHE}$ is the light harvesting efficiency, $\eta_{inj}$ is the electron injection yield from the photo-excited dye into $TiO_2$, and $\eta_{cc}$ is the charge collection efficiency at the electrodes. [22]

$$\eta = \frac{I_{sc}\, V_{oc}\, FF}{P_{in} A_{cell}} \qquad \text{(Equation 6)}$$

$$I_{sc} = q_c \int_{\lambda_{min}}^{\lambda_{max}} I_{photon}(\lambda)\, IPCE(\lambda) d\lambda \qquad \text{(Equation 7)}$$

$$IPCE\ (\lambda) = \eta_{LHE}\, \eta_{inj}\, \eta_{cc} \qquad \text{(Equation 8)}$$

## 2.4 The role of $TiO_2$ layer

The high surface area of the mesoporous metal oxide film is crucial for efficient device performance because it allows high absorption of solar irradiation by only a monolayer of adsorbed sensitizer dye. [21] When Tsubomura et al first introduced the concept of DSSC in *Nature* in 1976, they recognized that the poor photocurrents were primarily attributed to small quantity of dyes on the electrode surface. Tsubomura et al used a zinc oxide disk as a working electrode, but because of the smooth surface of the electrode layer, not enough dye molecules were adsorbed to give sufficient photocurrent generation. [15] Gratzel group resolved this problem by introducing mesoporous metal oxide film to increase the surface area, which would then increase the amount of adsorbed dyes on the surface substantially. On a flat surface, monolayer of dye absorbs at most a small percent of impinging light because it occupies an area that is several hundred times larger than its optical cross-section.[23] Other than $TiO_2$, other n-type materials with a wide bandgap semiconductor oxide, such as ZnO or $SnO_2$ were also investigated by various groups. However, $TiO_2$ is the most commonly used material because it is low-cost, widely available, non-toxic and bio compatible material. [23]

In order to optimize the capture of photons by dye molecules, a combination of $TiO_2$ layers with different nanoparticle size is utilized in DSSC. Generally, there are three types of $TiO_2$ layers for DSSC purpose: transparent layer, scattering layer, and reflective layer. Each type of layer is made with a different particle size of $TiO_2$, as shown in **Table 1**.

Table 1: Specifications of different types of $TiO_2$ layer [22]

| | **Transparent layer** | **Scattering layer** | **Reflective layer** |
|---|---|---|---|
| Particle size (nm) | 20 | 300-400 | 400-500 |
| General thickness (μm) | 5 ~ 20 | 4~5 | 4~5 |
| Purpose | Provide as much surface area as possible to adsorb dye molecules | Scatter incoming irradiation to prevent photons from escaping | Reflect scattered photons back to transparent layer |

Transparent layer is responsible for the majority of photon absorption. The high surface area is achieved through small particle size, and even with two or three layers of this type of nanoparticles can maintain high transparency. In order to maximize the dye molecule adsorption, the thickness of transparent $TiO_2$ layer should also be maximized. However, increasing the film thickness requires repeated layering of $TiO_2$ when processed through screen printing or solution casting (i.e. doctor blade method), which causes chances of surface cracking and increased internal resistance due to the molecular packing and thermal stress. The thickness of transparent $TiO_2$ layer must compromise with the internal resistance to find an optimal thickness.

As shown in **Figure 7**, scattering layer diffuses the incoming light as well as those reflected off of transparent layer or the conductive glass surface to capture photons within the $TiO_2$ layer. Sometimes additional layer of $TiO_2$ called reflective layer is applied in addition to the scattering layer, which reflects the diffused photons from scattering layer back to transparent layer. Due to the large particle size, scattering layer and reflective layer are translucent.

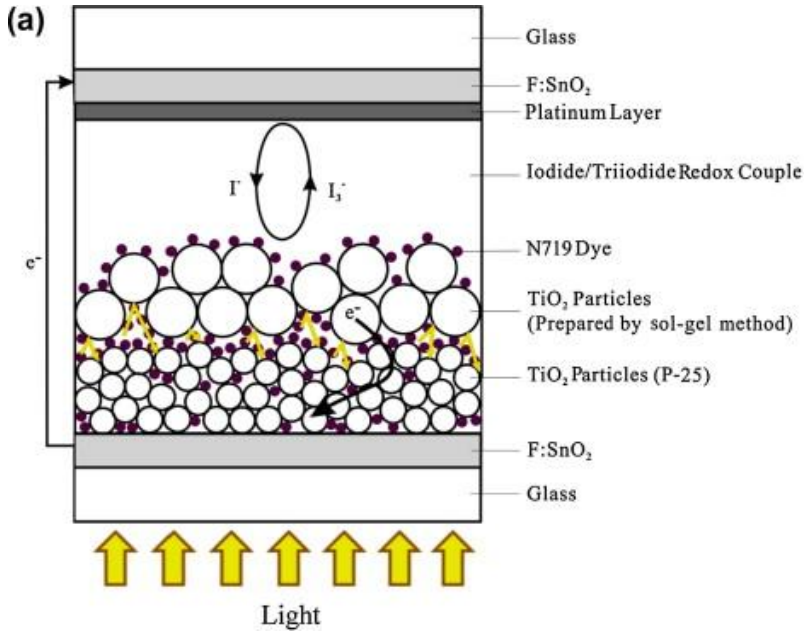


Figure 7: Schematic of DSSC showing two layers of TiO2 with different particle size[25]

Furthermore, depending on the molecular size of electrolyte couple utilized for DSSC, the porosity of $TiO_2$ film must correspond accordingly. For example, the size of $I^-/I_3^-$ redox mediators is in the order of atomic scales, so the porosity produced by the nanoparticle size of 20 nm is sufficient for the mediator ions to move through the layer. However, more bulky redox couple, such as $Co^{+3/+2}$ species would not fit through the pores of $TiO_2$ transparent layer. In such case, $TiO_2$ nanoparticle paste must contain different surfactant to increase the pore size of the resulting film.

## 2.5 Dye molecule

The molecular structure of dye molecules plays an important role in a DSSC performance. Ideally, dye molecule should have a broad range of absorbency spectrum, binds strongly to the $TiO_2$ semiconductor surface, has a suitably high redox potential for regeneration following excitation, and be stable over many years of exposure to sunlight. [26] As it was previously discussed, the energy levels of molecules determine its absorption range. From Equation 1, large

bandgap possesses absorption range in the longer wavelength (i.e. infrared region), and consequently the absorption range stays in UV region with small bandgap. However, the energy bandgaps of organic or organometallic materials usually fall within 2~3.5 eV, and the molecules become unstable outside of the range. LUMO and HOMO levels also need to match the conduction band of $TiO_2$ and redox potential of electrolyte couple, respectively; thus, the flexibility of the energy levels is rather limited. In reality, developing dyes with broad absorbency range, especially targeted at visible to infrared range because of its high intensity of irradiance (**Figure 8**) has been the biggest challenge of all. Considerable research has been conducted to shift the absorption range of dye molecules to near infrared region (NIR) to absorb increased amount of energy from solar spectrum.

As the photocurrent generation in DSSC sorely depends on the dye molecules, properties of dye molecules highly affect $I_{sc}$ (see Equation 7 and Equation 8) of the cell. Presently, highly efficient DSSCs were found to produce $\eta_{inj}$ and $\eta_{cc}$ close to 1; thus, the major strategy to improve $I_{sc}$ has been to improve $\eta_{LHE}$, which depends on the molar extinction coefficient of the dye, the amount of dyes anchored on $TiO_2$ film, and the optical path length of incident light within the dye-sensitized film. [22]

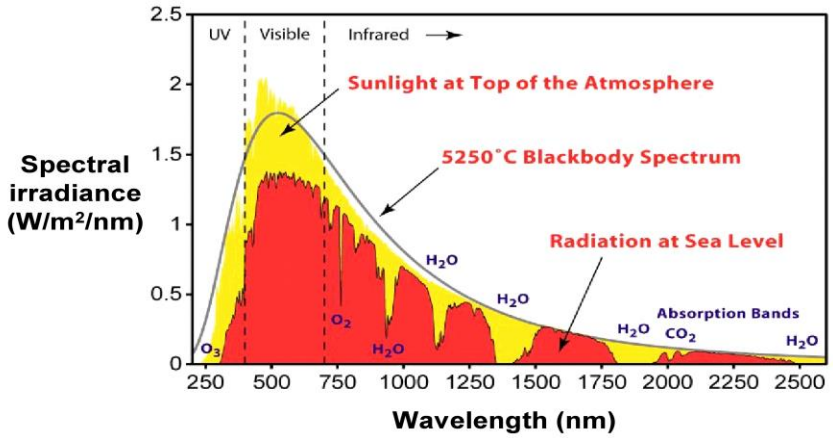


Figure 8: Solar irradiation spectrum at AM 0 [27]

Myriad of dyes have been developed thus far, including metal-organic complexes, organic compounds, Zn porphyrins, and Zn phthalocyanines. [22] In the following section, metal-organic complex (Ru based dyes) and organic dyes will be focused in the discussion as they are the two most promising groups of sensiziers for DSSC.

### 2.5.1 Ru polypyridyl complex

The most widely implemented dye is an organometallic Ruthenium dye: $RuL_2(NCS)_2$ complex (N3, red dye) and the $RuL(NCS)_3$ complex (N719, black dye), Both dyes are capable of absorption in a broad visible range, approximately 400 to 900 nm[28]. Although these two sensitizers are highly efficient, Ru is a rare metal, thus not suitable for future mass production of DSSCs.

Discovered in 1993 by Gratzel group[29], the photovoltaic performance of N3 dye was not unmatched until 2001, when they developed the "black dye" achieved a 10.4 % (AM 1.5) of PCE in full sunlight.[18] The chemical structures of the most efficient dyes are shown in **Figure 9**. This record was further renewed in 2008 again by Gratzel group, presenting 11.3 % efficient device with volatile acetonitrile-based electrolyte through the use of heteroleptic ruthenium complexes bearing alkylthiophene blocks conjugated with the bipyridine ligand, also known as C101 dye. [30] The greatest advantage of the heteroleptic complexes is that their extinction coefficients are almost 3 times higher than that of a typical black dye. This allows the device to reduce the thickness of $TiO_2$ film, resulting in higher open circuit voltage ($V_{oc}$) values because of a decrease in the dark current and increase in the electron concentration.[31]

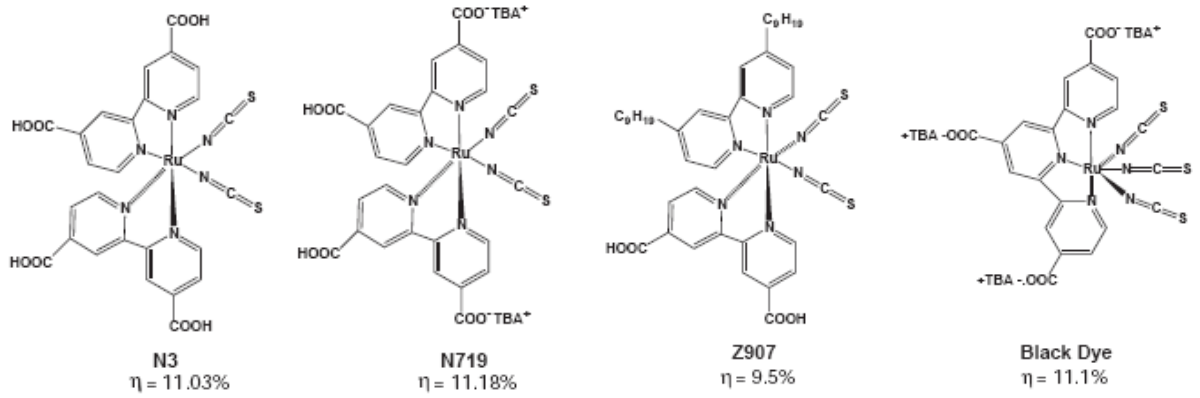


Figure 9: Structures of some of the most efficient Ru polypyridyl complex dyes for DSSC [32]

### 2.5.2 Organic dyes

Recently, interests in organic dyes have been blooming to compete with the efficiency of Ru based dyes. Organic dyes are considered promising sensitizers for DSSCs due to the high molar extinction coefficient, low cost, rare metal free, and high design flexibility of the molecules.[22] They are different from Ru based dye with its structure and thus the electron transfer mechanism. They are also thought to have efficient and rapid electron injection from the excited state of the sensitizer into the conduction band of the metal oxide, [9] where many adopt the donor-π-conjugation (linker)-acceptor structure such as shown in **Figure 10**. Donors are composed of electron-donating moieties, whereas acceptors are composed of electron-accepting moieties. As the photogeneration occurs in the dye molecule, electron will be efficiently transferred from donor to acceptor group, where acceptor injects electron to $TiO_2$ through carboxylic acid bonding. Organic dyes results in a high extinction coefficients compared with Ru based dye, which is advantageous in DSSCs with ionic liquid or solid-state hole conductor, because they allow good light harvesting efficiencies using thinner $TiO_2$ films.[31] Other benefits of organic dyes include abundance in raw materials, large absorption coefficient due to intermolecular π-π* transitions, and large variation in structure with facile modification.[24]

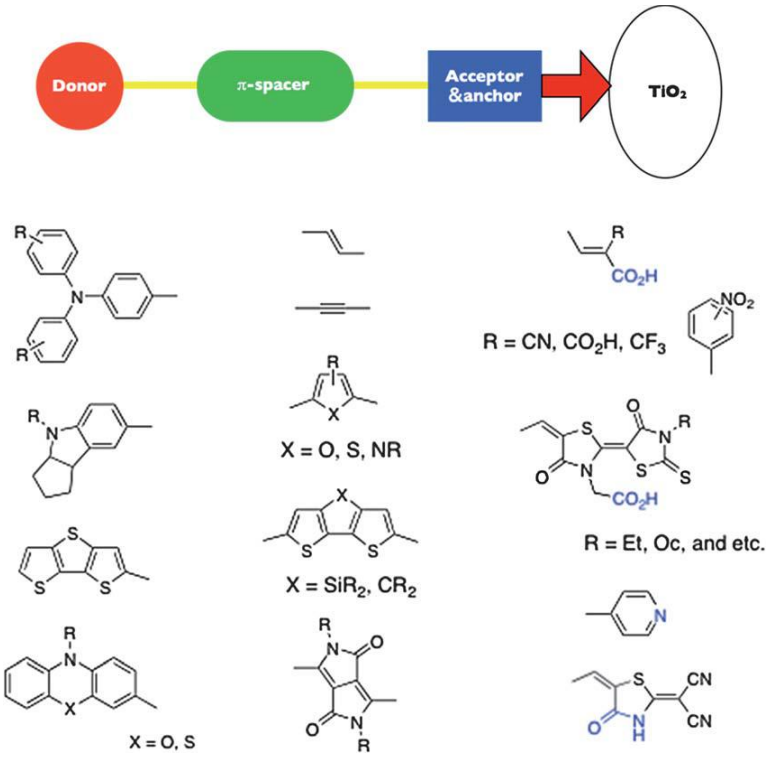


Figure 10: Schematic drawing of D-π-A type organic dye and some samples of the donor, π-spacer and acceptor with anchoring (in blue) components [22]

## 2.6 Redox couple for electrolyte

The important properties of electrolyte solution include redox potential of the redox component (often referred to as mediators), ionic conductivity, and corrosivity of the mediators. The difference between the quasi-Fermi level of electrons in $TiO_2$ under illumination and the redox potential of the mediators determines the maximum open circuit voltage of the DSSC [20] (dotted line on Figure 6), while the redox potential should be above and as close as possible to the HOMO level of the sensitizer for efficient regeneration of oxidized sensitizers. The ionic conductivity indicates the ion movement in the cell, which is determined by the electrolyte solvent and mediator components in use. Lastly, corrosivity of the mediators pose issues with the lifetime of the DSSC, since sealant of the cell must be compatible with the chemical composition of the mediators.

Both in DSSC's first appearance in *Nature* 1976 and Dr. Gratzel's paper in 1991, electrolyte contained the $I^-/I^{3-}$ as a redox couple.[16,17] With its sufficiently large redox potential, iodine electrolyte is still widely used for DSSC, but iodine has three major drawbacks. One, $I^-/I^{3-}$ system is limited by its relatively high overpotential for dye regeneration. In an electrolytic cell, the overpotential requires more energy than thermodynamically expected to drive a reaction. Secondly, triiodide also absorbs photon competitively. Lastly, $I^-/I_3^-$ is corrosive toward most metals and sealing materials and its solvent being acetonitrile (i.e. votalile) decreases the durability of the overall cell.[31] To overcome these challenges, there have been two main approaches: alteration of solvent, and the development and the use of iodine-free redox couple.

### 2.6.1 Electrolyte solvents

Acetonitrile is a favorable electrolyte solvent in DSSC, but it is volatile and toxic, has high vapor pressure, and is relatively rare organic solvent, which gives incentives to find alternatives. There are numerous reports on gelation of electrolyte to reduce evaporation of solvent, but the highest efficiency obtained with gel electrolyte is 7.18 %,[32] where the value still cannot compete with the liquid electrolyte record due to its reduced electron mobility (**Table 2**). The use of ionic liquid is becoming more common, but ionic liquid has a high viscosity thus low efficiency, and has high processing cost. However, imidazolium iodide, an ionic liquid revealed very attractive stability features. Despite its high viscosity, overall PCE exceeding 6 % has been observed.[33] This has been attributed to a Grothus mechanism which increases the diffusion coefficient of the triiodide ions in the melt and to a very effective mode of charge screening, which is operative in this ionic liquids. [9] Additionally, these solvents were replaced by highly polar and nonvolatile solvents, such as methoxypropinitrile (MPN). A DSSC device with MPN based electrolyte in conjunction

with a surfactant ruthenium dye recently passed the critical 1000 h stability test at 80 °C, which was the first time with a DSSC.[34]

Table 2 Advantages and disadvantages of liquid and gel (ionic liquid) solvent for DSSC electrolyte

| Electrolyte | Advantages | Disadvantages |
|---|---|---|
| Acetonitrile (liquid) | • Provide fast diffusion rate for iodine<br>• Low viscosity<br>• Low cost | • Volatile<br>• Low long-term stability<br>• Flammability |
| Ionic liquid (chemical gel) | • Non-volatile<br>• Non-flammable<br>• High ionic conductivity<br>• Thermal and chemical stability<br>• Fast exchange-reaction of an iodine | • High viscosity<br>• High cost<br>• 80 % of the Jsc of the DSSC with standard electrolyte solution with acetonitrile |

### 2.6.2 Emerging alternative to iodide/triiodide redox couple—Cobalt redox couple

There are numerous alternative redox couple that has a potential to substitute iodide/triiodide couple, such as $Co^{+3/+2}$ system[31], an alkali metal polysulfide ($S_n^{2-}/S_{n+1}^{2-}$), and a cesium thiolate salt (disulfide/thiolate) [35]. Out of all the alternative redox couple for iodide/triiodide, the most promising couple up to date is $Co^{+3/+2}$ system. Cobalt based redox couple has numerous advantages over that of iodine. It has less competitive absorption at visible light region, less corrosive toward metals, and its redox potential can be easily tuned through varying ligands. **Figure 11** shows the varying redox potential through substituents at –R of $[Co(bpy)_3]^{3+/2+}$ couple. Today, the highest efficiency achieved with $Co^{+3/+2}$ is 12.3 % under AM 1.5 global sunlight, coupled with porphyrin-based dye sensitizers.[36] This record demonstrated the effectiveness of cobalt redox couple for DSSCs, as long as dyes with suitable characteristics were couple together.

However, $Co^{+3/+2}$ system has a number of drawbacks. Firstly, its dye regeneration rate is slower than that of $I^-/I_3^-$ couple. Secondly, $Co^{+3/+2}$ redox reaction involves only one electron; thus, the recombination with $TiO_2$ and/or FTO occurs at much faster rate. Also, due to the bulkiness of cobalt complex, diffusion of cobalt ions are very slow, which is known as mass transfer problem.

[37] Numerous measures can be done to mitigate these problems, such as application of passivation layer and dye design with a blocking layer, which will be discussed in the following section.

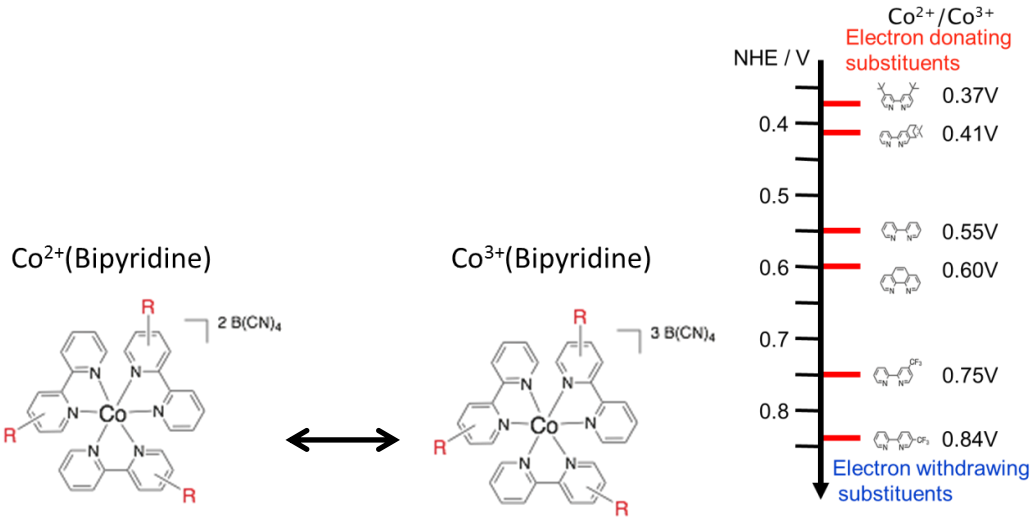


Figure 11: Co(bipyridine) (III)/(II) chemical structure and alteration of redox potential through substituents at –R (Image courtesy of Nobuyuki Yoshida, Shinshu University)

### 2.6.3 Recombination process in DSSCs

Under illumination, spontaneous reactions such as photogeneration by dye molecules push the cell away from equilibrium. In response, recombination reactions compete to drive the cell back to equilibrium. There exist three recombination pathways: [37]

1. $e_{TiO2}$ with oxidized dye (Figure 12, 1)

$$e_{TiO_2} + D^+ \rightarrow D$$

2. $e_{TiO2}$ with oxidized redox (Figure 12, 2)

$$e_{TiO_2} + R^+ \rightarrow R$$

3. $e_{SnO2}$ with oxidized redox

$$e_{SnO_2} + R^+ \rightarrow R$$

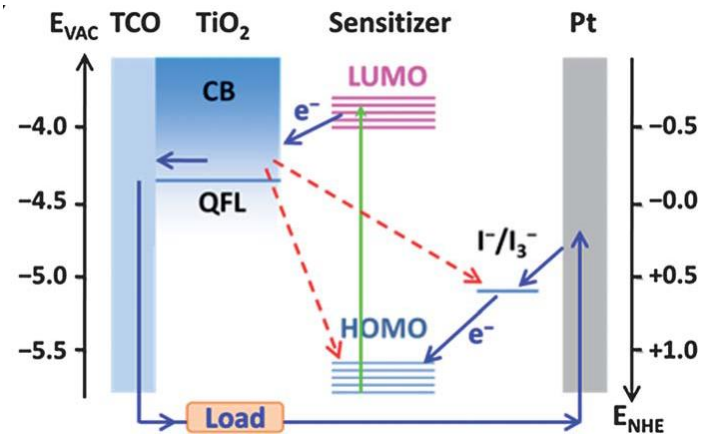


Figure 12: Reactions in DSSC upon illumination [22]

The 3rd recombination pathway (not shown in **Figure 12**) exists because $TiO_2$ does not entirely cover the FTO surface. [38] Whether the recombination plays a significant role in DSSC depends on the kinetic rate of the following reactions: dye regeneration rate and recombination rate. Dye regeneration occurs between dye molecules and electrolyte redox couple; oxidized dye from photoexcitation is regenerated by oxidizing agent of redox couple. The kinetic rate of recombination is a characteristic of redox couple. As for the recombination rate of redox couple, the number of electrons involved in the redox reaction is the determining factor. For example, the redox reaction that involves one electron ($Co^{+3/+2}$) is faster than that of two electrons ($I^-/I_3^-$), and those with smaller redox species are superior in mass transfer speed. [38]

The recombination process is generally suppressed by application of passivation layer, and building a blocking layer (electron-donating group) into the dye structure. For the application of passivation layer, ultrathin aluminum layer or $TiCl_4$ layer is applied to $SnO_2$ and/or $TiO_2$ to block the electron transfer from those layers to oxidized dye or oxidized redox specie. Integration of blocking layer in dye design has been proven to be effective especially for $Co^{+3/+2}$ couple electrolyte, because its dye regeneration rate is slower than that of $I^-/I_3^-$ couple.[39] **Figure 13**

shows three TPA-backbone based dyes, where D29 and D35 incorporates electron-donating substituents, *p*-*N*,*N*-dimethylanilinyl and *o*,*p*-dibutoxyphenyl, respectively. The influence of recombination is obvious in **Figure 14**, when TPA-4 mounted DSSCs were fabricated with $I^-/I_3^-$ couple and $Co^{+3/+2}$ couple. While passivation layers were applied to both $SnO_2$ and $TiO_2$ on all cells, lack of blocking layer on dye molecules resulted in recombination from $TiO_2$ to $Co^{+2}$ species, which inhibited direct electron transfer from $TiO_2$ to $SnO_2$.

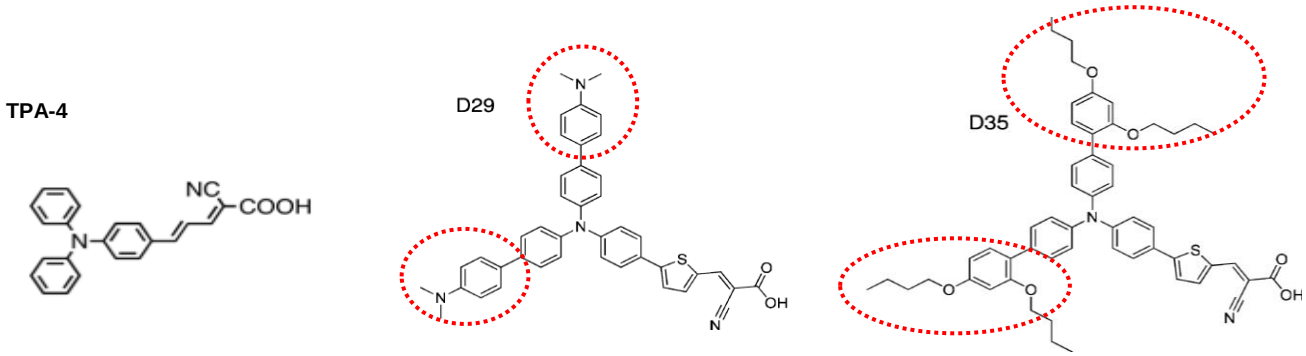


Figure 13: Three TPA-backbone based dyes, TPA-4, D29, and D35. Red dotted line shows the recombination blocking groups

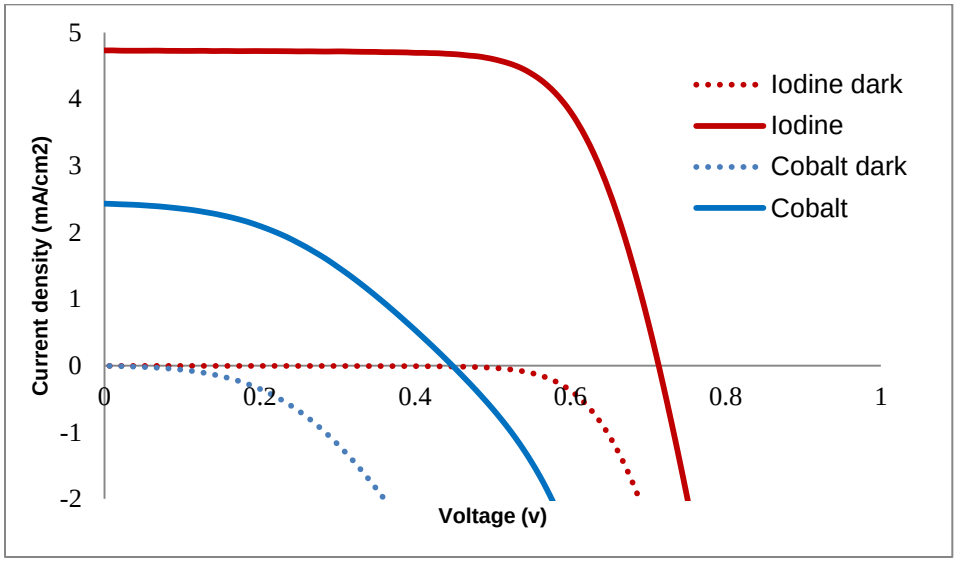


Figure 14: I-V properties of TPA-4 with iodine and cobalt electrolytes

Table 3: I-V properties of TPA-4

| Electrolyte | Voc [V] | Jsc [mA/cm2] | FF | PCE [%] |
|---|---|---|---|---|
| Iodine | 0.71 | 4.73 | 0.71 | 2.41 |
| Cobalt | 0.45 | 2.43 | 0.42 | 0.46 |

## 2.7 Counter electrode

The role of counter electrode (CE) in DSSC is necessary to reduce redox species in the electrolyte, which ultimately connects to the regeneration for the sensitizer after electron injection (Figure 6 and Figure 12). In order to optimize the performance of DSSC, CE material should possess the lowest possible sheet resistance, high catalytic activity for the reduction of the redox electrolyte, and high chemical stability. [20]

The most commonly employed counter electrode material is Pt for its excellent catalytic activity and high corrosion stability against the widely employed iodine electrolyte. The platinum thin film is processed through sputtering or sol-gel (doctor blade or simple solution application), where the surface area of Pt correlates with its catalytic activity. However, the high cost of Pt due to global demand of Pt has been one of the limiting factors of the widespread of DSSC. Numerous materials were explored in a search of alternatives to Pt: [19] graphene, transition metal sulfides, nitrides, carbides, and conductive polymers. By far, there is no promising substitute that exhibits the properties of Pt with $I^-/I_3^-$.

# Chapter 3: Energy-Harvesting Electrochromic Window

## 3.1 Introduction

Electrochromic window (ECW) is an emerging dynamic window technology that actively controls the transmittance of light upon modest applied potential. While ECW has a great potential for energy saving from heating and cooling in buildings, automobiles, and aircrafts, energy harvesting function is ideal to self-power the system and advance in energy conservation.

## 3.2 Different types of self-powered ECW

There are three types of self-powered ECW designs reported thus far: side-by-side (horizontally integrated), [40] tandem (vertically integrated through the window thickness direction), [38, 41] and photoelectrochromic (PEC). [42-44] Side-by-side design locates photovoltaic devices around the edges of ECW. There will always be tradeoffs between the window area and power generated by PV in this design. Tandem device places ECW behind solar cell, thus it does not conflict the area of window and solar cell; however, such design lacks transparency, since photovoltaic cells require absorption at visible range to generate sufficient photocurrent. Tandem design also significantly increase the device thickness and experience energy loss upon energy transfer from one cell to another, which makes it unrealistic for practical application.

Among the three designs, PEC device is the most economical, efficient, and promising for practical use due to its monolithic design, where two functional thin films (i.e. electrochromic and photovoltaic) are integrated into one electrochemical cell (**Figure 15**). PEC devices are designed as a combination of a dye-sensitized solar cell (DSSC) [16, 17] electrodes and an electrochromic film on either side of the electrode. [43] In DSSC, unlike conventional photovoltaic cells where a built-in electric field separates the photogenerated charge carriers to produce the photocurrent, the charge separation process is almost entirely kinetically controlled, rather than

driven by an electric field. [19] On the other hand, ECW performs electrochromism upon intercalation and deintercalation of mobile ions driven by externally applied electric field. Thus, integration of electrochromic film within DSSC device allows kinetically controlled demonstration of electrochromism, which makes combination device such as PEC possible.

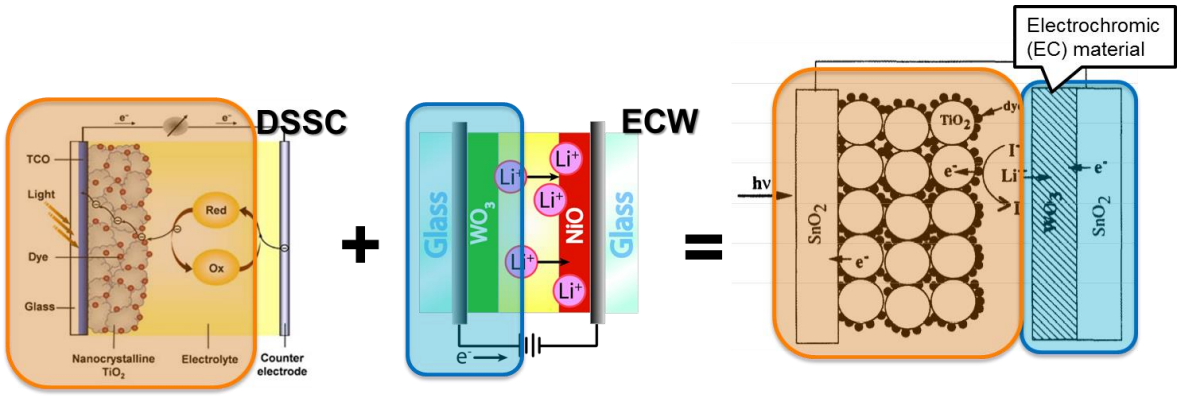


Figure 15: Schematic figure of photoelectrochromic device

### 3.3 Reported studies on PEC device

Although the mechanisms of ECW and DSSC are complementary, several features conflict the properties of one another to achieve efficient self-powered ECW. Firstly, the nature of DSSC requires sensitizer to absorb light in the range of visible wavelength to generate sufficient photocurrent; however, such absorption pattern leads to the lack of transparent state of the device, thus not suited for window applications. The absorption at the electrolyte of DSSC also raises the same issue of transparency. $I^-/I_3^-$ redox couple is a widely accepted redox couple for DSSC electrolyte, but has a very competitive absorption at visible range, i.e. dark color. Most studies of PEC device utilizes $I^-/I_3^-$ couple, except Hsu et al who evaluated numerous redox couples on the photovoltaic and electrochromic properties of a PEC device with poly (3,4-(2,2-diethylpropylenedioxy)thiophene) (PProDOT-$Et_2$) and a thienylfluorene conjugated organic dye. The highest contrast ratio was observed with $Br^-/Br_3^-$ redox couple, with $T_{max}$= 45.3 % and

$T_{min}$=11.6 % of transmittance at bleached and colored state, respectively; however, the photovoltaic efficiency observed in terms of power conversion efficiency (PCE) was very small, 0.14 % (50 mW $cm^{-2}$). [45] Furthermore, they did not discuss the electrochemical stability of PEC device over cyclic operation. One cyclic durability test of PEC device known to the authors is the study by Yang et al, where a PEC device is based on electrochromic polymer, poly (3,4-(2,2-dimethylpropylenedioxy)thiophene) (PProDOT-$Me_2$) thin film and Pt layer on counter electrode with ruthenium dye DSSC. They demonstrated reasonable stability of the PEC after 1500 cycles, no major change in electrochromic property other than increase in bleaching speed was observed, but the PCE value reported is 1.12 % (100 mW $cm^{-2}$) [46]. Wu et al also performed the cyclic stability test on the PEC device consisted of patterned $WO_3$/Pt electrochromic electrode as counter electrode of DSSC with N719 dye, which exhibited 0.5 % PCE with the transmittance of 50 % and 10 % at bleached and colored state, respectively at 788 nm. [47] This study stated good cyclic stability in electrochromic property after 200 cycles, but the cyclic durability of photovoltaic property was again not discussed.

Most of the existing PEC devices are passive, not controllable externally, while active PEC system is desired to fully benefit the dynamic control feature of ECW. Wu et al [47] realized tunable transmittance under illumination through the integration of variable resistor in series with the cell, but its performance depends on the presence of illumination. The ideal design of self-powered ECW utilizes illumination for photovoltaic purpose only, and the device transmittance should be controlled actively from external source. The only reported design of such device is a DSSC with co-adsorbed ruthenium based dye and electrochromic dye [48] where PCE of1.1 % under 0.1 Sun (10 mW $cm^{-2}$) and a transmittance change from 38.7 % (bleached) and 15.9 % (colored) were presented. The co-adsorption design uses $TiO_2$ electrode for photovoltaic and

electrochromic properties, which requires compromise between the two properties. All the past examples of self-powered ECW discussed here are summarized in **Table 4**.

Table 4: Summary of published results on self-powered ECW

| Source (ref) | Dye | $TiO_2$ (μm) | Area (cm2) | Redox couple | EC material | Jsc (mA/$cm^2$) | Voc (V) | FF | PCE (%) | $T_{max}/T_{min}$ | ΔT | λ (nm) | Illum. (mW/cm2) | Switch speed (c/b) | Cyclic Durability |
|---|---|---|---|---|---|---|---|---|---|---|---|---|---|---|---|
| 41 | Ru | 7 | 24 | $I^{3-}/I^-$ | WO3 | 3.96 | 1.35 | 0.54 | 2.9* | 36.7/1.2 | 35.5 | 750 | 100 | 60/45 | N/A |
| | organic (FL dye) | ? | 1 | Br-/Br3- | PEDOT | 0.89 | 0.57 | 0.64 | 0.65 (50mW/cm2) | 24.7/10.6 | 14.1 | 620 | 50 | 3/3 | N/A |
| 45 | organic (FL dye) | ? | 1 | $I^{3-}/I^-$ | PEDOT | 0.12 | 0.66 | 0.9 | 0.14 (50mW/cm2) | 45.3/11.6 | 33.7 | 620 | 50 | 96/36 | N/A |
| 47 | Ru (N719) | 3 | 1.44 | $I^{3-}/I^-$ | Patterned $WO_3$ with Ag | 2.23 | 0.57 | 0.4 | 0.5 | 53/10 | 43 | 788 | 4 | <1/4 | 200 |
| 45 | Ru (535-4TBA) | 1 | 4 | $I^{3-}/I^-$ | Pt+ PProDOT-$Me_2$ | 2.92 | 0.66 | 0.58 | 1.12 | 47/9 | 38 | 637 | unknown | 4/1 | 1500 |
| 48 | Ru and viologen | 3 | 1 | $I^{3-}/I^-$ | Viologen | 0.67 | 0.27 | 0.62 | 1.1 | 38.8/20 | 18.8 | 630 | 10 | 0.6/0.6 | N/A |

## 3.4 Our proposed design of EH-ECW

In this study, we present a new design of self-powered electrochromic window called energy-harvesting electrochromic window (EH-ECW) that exhibits high photovoltaic performance, actively tunable transmittance through modest applied potential, fast-switching rate, and robust cyclic durability of both electrochromic and photovoltaic properties over 5000 cycles. In order to retain both electrochromic and photovoltaic performances of the EH-ECW device without sacrificing one another, $Co^{+3/+2}$ redox couple was chosen over the standard iodine redox couple. Owing to its high redox potential, $Co^{+3/+2}$ couple can provide higher open circuit potential ($V_{oc}$) compared to $I^-/I_3^-$. $Co^{+3/+2}$ couple has not only proven to be as efficient as $I^-/I_3^-$ couple when accompanied with articulately designed organic dye to reduce recombination at titania surface, [36] it also has less competitive absorption at visible region, which allows increased transparency of the electrolyte component in this newly designed EH-ECW. $Co^{+3/+2}$ couple also bring advantages

from its compatibility with conductive polymers as counter electrode. While the charge transfer of $I^-/I_3^-$ is best performed with Pt catalyst counter electrode due to platinum's capability of forming charge-transfer with $I_3^-$, $Co^{+3/+2}$ couple exhibits excellent compatibility with conductive polymers. [49] Tsao et al [50] found that cobalt redox shuttles exhibited lower charge transfer resistance at counter electrode when employed with PEDOT compared to Pt, this lower charge transfer was achieved by the porous, three dimensional electro-active morphology of PEDOT.

The high extinction coefficient of organic dyes allows retaining photocurrent generation even with thin $TiO_2$ layer. Thin $TiO_2$ layer not only simplifies the fabrication process, but is also advantageous to increase transparency of the overall device, and overcome the mass transport and recombination issue of $Co^{+3/+2}$ couple. The color of the sensitizer is easily tunable through the modification of molecular structure with organic dyes. Additionally, unlike the conventional PEC device, EH-ECW performs electrochromism through externally applied potential. Although this feature allows active control of transmittance through varying applied potential, such electrochemical process is expected to damage components of the EH-ECW device. Specifically, the coordinate bonding between dye monomers and $TiO_2$ is expected to break, resulting in dye desorption. We propose to overcome this by integration of polymeric sites to the dye molecules, allowing the dye monomers to polymerize on the surface of $TiO_2$ under cyclic applied potential.

One idea for the application of EH-ECW in residential buildings as an integrated smart window system is shown in **Figure 16**. Since the visibility of the top area of window is unnecessary for practical use, such area can mount semi-dark colored DSSC (shown as W1) to harvest energy. The middle area, which is at the average eye level, may embed EH-ECW (W2). ECW can be installed at the bottom area of the window, which of its operation energy may be supplied by

energy harvested by W1. This multifunctional window allows users to adjust the transmittance at the level of their eye level for visual comfort, while self-supply energy for its functions.

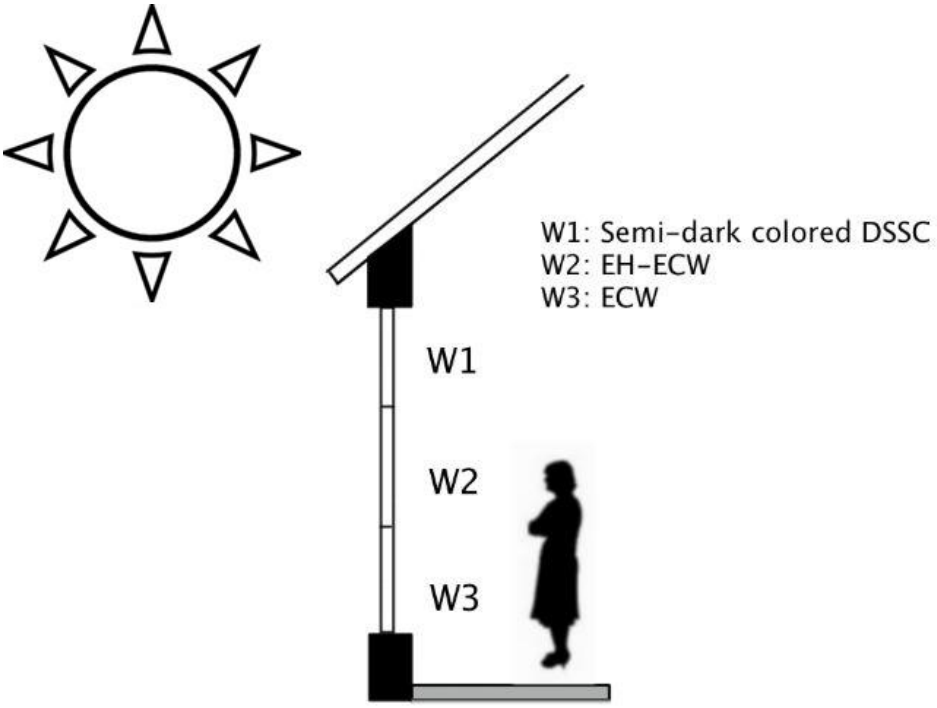


Figure 16: Schematic of multi-design integrated smart window for residential windows.

# Chapter 4: Materials and Methodology

## 4.1 Materials Synthesis and Characterization

### 4.1.1 Molecular design of polymeric dye

Conventional DSSC mounts ruthenium based organometallic dyes, which exhibit broad absorption range by means of metal to ligand charge transfer. However, ruthenium dyes have two major drawbacks: dark color and low molar absorption coefficient. In order to achieve high photocurrent generation, thickness of the $TiO_2$ film is often maximized to increase the amount of adsorbed dye molecules. Since the thickness of $TiO_2$ film must be minimized to achieve high transmittance in EH-ECW device, organic sensitizers are chosen for their high molar absorption coefficient through $\pi$- $\pi^*$ transition, comparable efficiency to organometallic dyes, and facile tunability of the dye color by molecular structural design. With these advantages, high transmittance and high photovoltaic performance can be made possible without a sacrifice of one property to another.

In order to obtain high efficiency and durability upon adsorption in EH-ECW, triphenylamine (TPA)-based organic dyes with polymeric site [51] were selected and synthesized in this study. Carboxylic acid was introduced as an anchoring group, and polymeric sites were introduced through inclusion of two thiophene rings. A number of functional substituents were added to thiophenes to optimize the resulting molecular structure with efficient electron transfer. Unlike iodine ions, cobalt ions are cations; thus, sensitizer structure must contain alkyl chains to prevent cobalt cations from being drawn toward $TiO_2$ to proceed with recombination. [52] With such consideration in mind, SA8 and SA13 were designed and synthesized with hexyl chains added to the 3$^{rd}$ and 4$^{th}$ position, respectively; see **Scheme 1**. Detailed results on the material characterization of the synthesized SA8 and SA13 are included in Appendix A. Gaussian

computation of SA8 and SA13 confirms delocalization at the TPA backbone to the thiophene polymeric unit in HOMO level, and LUMO is delocalized at the carboxylic acid anchoring group **(Figure 17**). Efficient electron transfer from donor to acceptor site of the molecules is anticipated, and good charge separation from an occupied orbital of the LUMO prompts electron injection to $TiO_2$. We also synthesized D35, known efficient organic dye when coupled with cobalt electrolyte, through following the work by Hagberg et al [52] as a comparison.

The energy levels of SA8 and SA13 were computed using cyclic voltammetry (electrolyte: 0.1 M tetrabutylammonium perchlorate in acetonitrile) results as well as differential pulse voltammetry with ferrocene correction. As shown in **Figure 18**, there was no large difference in the energy levels of SA8 and SA13. The LUMO levels of both SA dyes were found to situate right above the conduction band of $TiO_2$, ensuring efficient electron injection. The HOMO levels were also suited with the redox potential of $[Co(bpy)_3]^{3+/2+}$ couple, [39] where regeneration of oxidized dyes can be achieved, The photovoltaic properties of DSSC with each developed sensitizer $[Co(bpy)_3]^{3+/2+}$ couple and Pt counter electrode reflect the energy level results. The DSSC with SA13 dye (SA13) exhibited the highest power conversion efficiency of 4.5 % ($V_{oc}$ = 0.74 V, $J_{sc}$ = 8.5 mA/cm$^2$, FF = 0.72) (**Figure 19**). The higher performance of the DSSC with SA13 relative to that of SA8 is attributed to the insertion of hexyl chain on the position far from the TPA backbone, which allowed expansion of alkyl chains and thus resulted in improvement of $V_{oc}$. The bond angle between TPA and alkyl chains was also reduced; the improved $J_{sc}$ is a result of the extension of conjugation length. The aggrandized structure of SA13 is thought to have achieved a better recombination blockage against the flow of cobalt cations from $TiO_2$. This interpretation of the result is also supported by the dark state of current-voltage measurement,

where the slope of dI/dV of the EH-ECW with SA13 is the smallest among the three compounds synthesized.

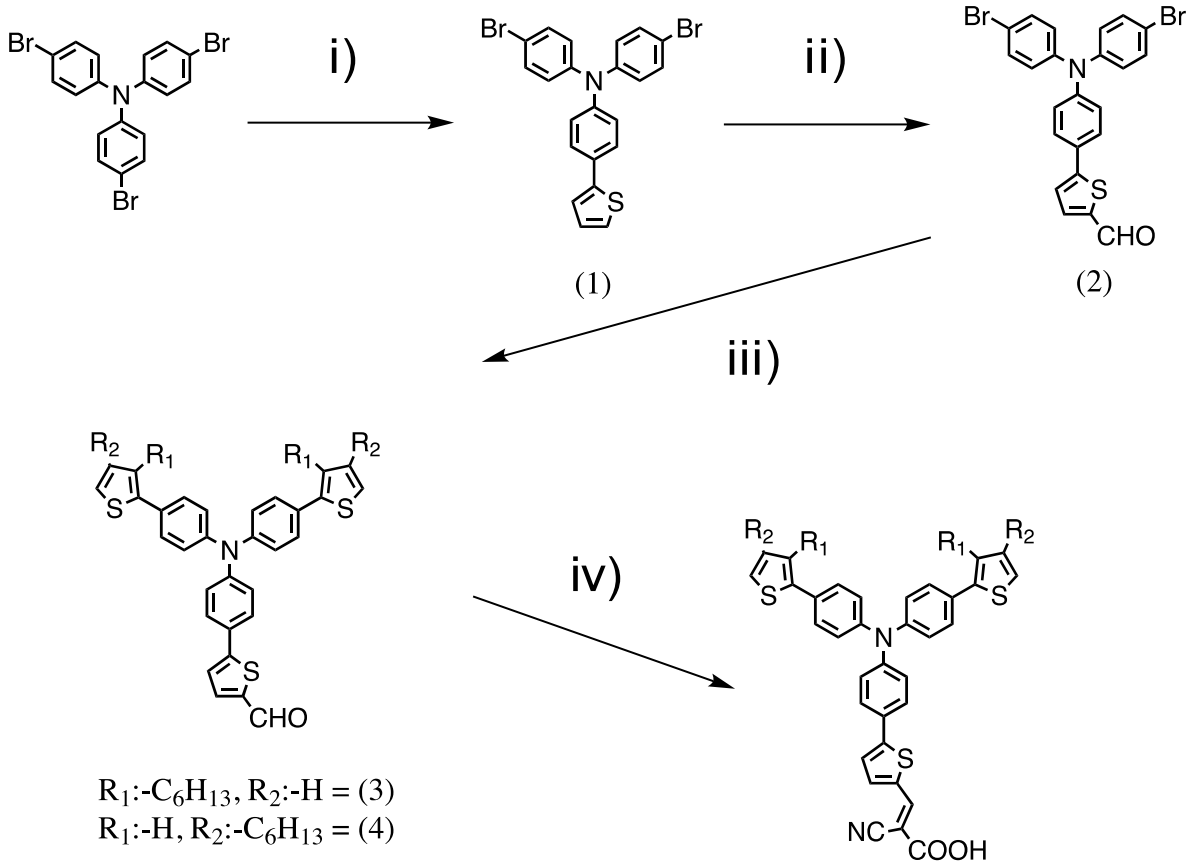


Scheme 1: Synthesis of SA13. Reagent and experimental conditions: (a) 2-thiophenebromic acid, Pd(PPh3)4, THF, 2.0 M aqueous K2CO3; (b) POCl3, dry-DMF; (c) THF, toluene, 2.0 M aqueous K2CO3, Pd(PPh3)4, 4-hexyl-2-(4,4,5,5-tetramethyl-1,3,2-dioxaborolan-2-yl)thiophene; (d) cyanoacetic acid, piperidine, dry-acetonitrile, dry-toluene.

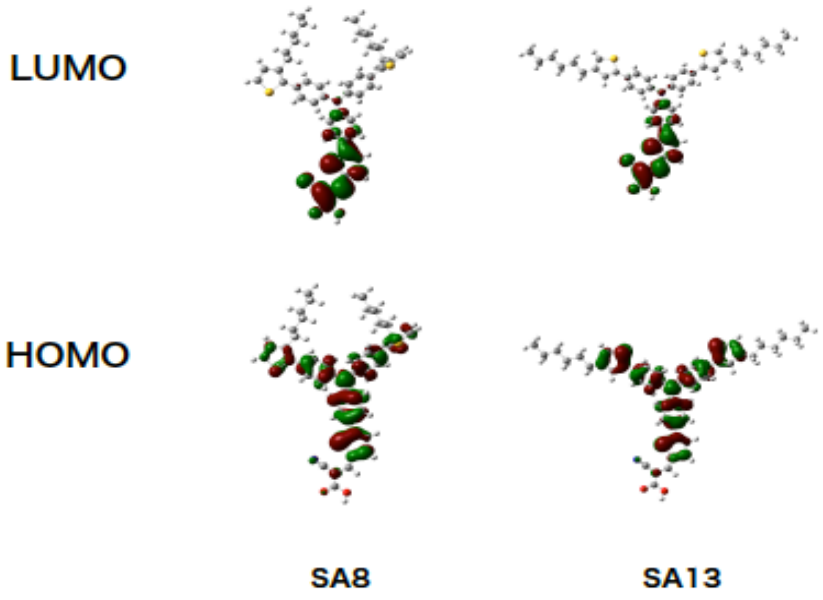


Figure 17: Isodensity surface plots of the HOMO and LUMO for SA8 and SA13

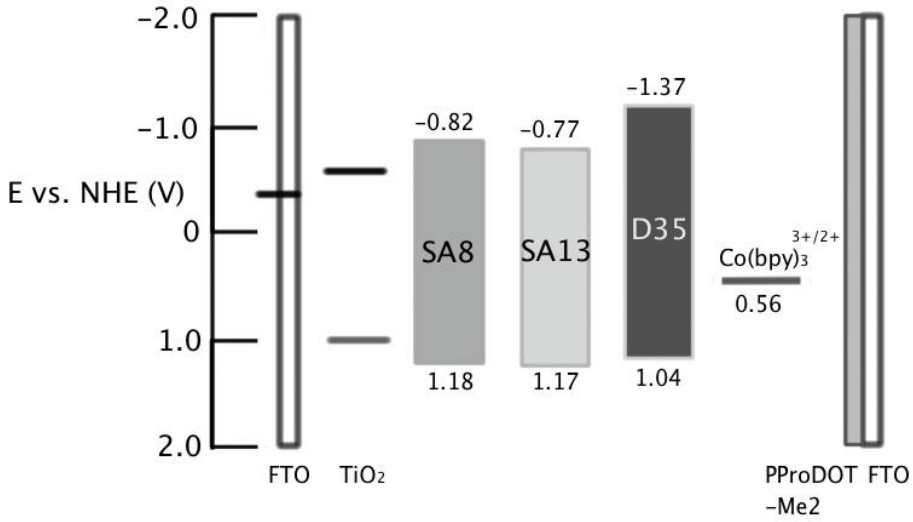


Figure 18: Schematic energy diagram of EH-ECW comparing the three dyes evaluated: SA8, SA13, and D35, where the HOMO and LUMO values of D35 was taken from Hagberg et al [51]

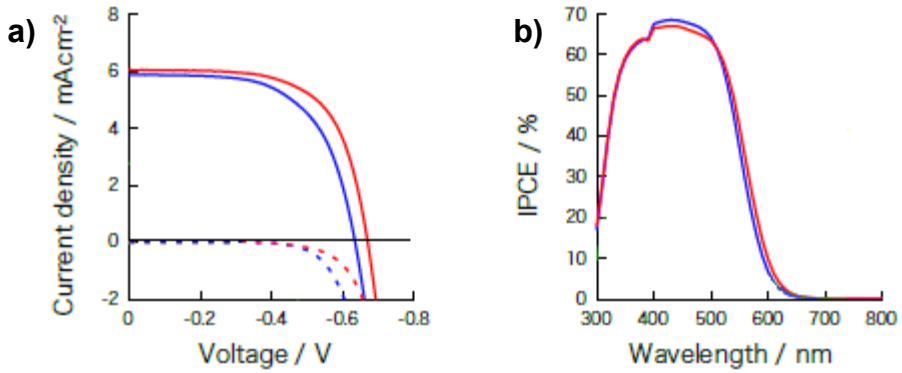


Figure 19: a) I-V curve of DSSC with SA8 (blue) and SA13 (red) and b) IPCE of those cells

### 4.1.2 Electropolymerization phenomenon of polymeric dye

The physical effect on the dye molecules, whether or not the molecules remained adsorbed on the surface of $TiO_2$ or the structural change induced by electric field was evaluated through comparing the absorbance of dye adsorbed $TiO_2$ electrode at every 100 cycles up to 300 cycles of +1.5 V and 0 V with the period of 10 seconds in 0.1 M tetrabutylammonium perruthenate in acetonitrile. The intensity of D35 absorbance peak in UV-Vis spectra is reduced after 100 cycles (**Figure 20b**); since the absorbance results are not normalized, quenching of absorbance intensity directly implies dye molecule's detachment from $TiO_2$ surface or molecular structural destruction. On the other hand, SA13 shows a red shift after 100 cycles (**Figure 20a**), indicating stabilization of dye molecules through electropolymerization from applying cyclic potential. To further evaluate the polymerization process of dye molecules, cyclic voltammetry (CV) tests were conducted on dye adsorbed $TiO_2$ film. The CV test results of SA13 show changes in oxidation peaks after the second cycle (**Figure 20c**), which indicates the progression of oxidative polymerization of the thiophene through the activation of the $2^{nd}$ (and $5^{th}$) position from applying positive electric potential. In contrast, the waveform of CV test results of D35 substrate (Figure 20d) remained unchanged over time; no structural change occurred under electric field. Thus,

inclusion of thiophenes to the molecular structure made the polymerization of dye molecule (namely, SA13) on the surface of $TiO_2$ nanoparticles possible.

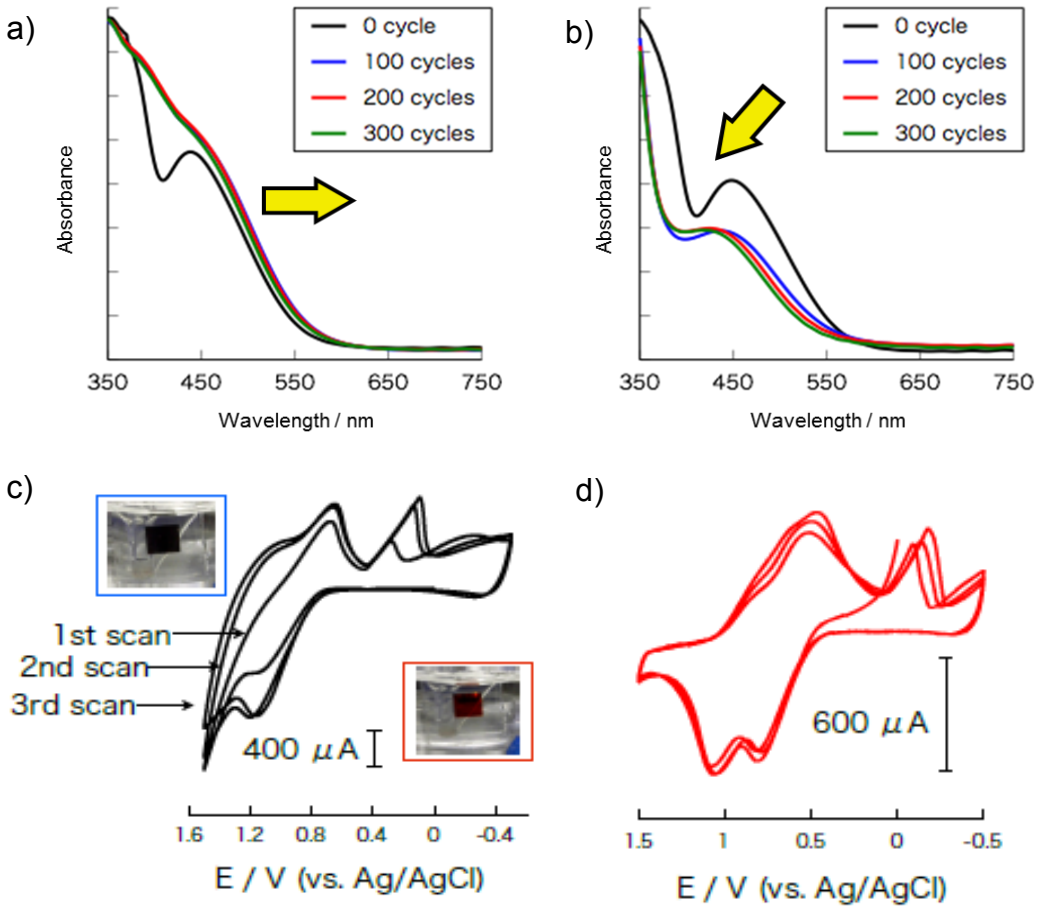


Figure 20: Absorbance spectrum of cyclic test of +1.5V with (a) SA13, (b) D35, and cyclic voltammetry of (c) SA13 and (d) D35

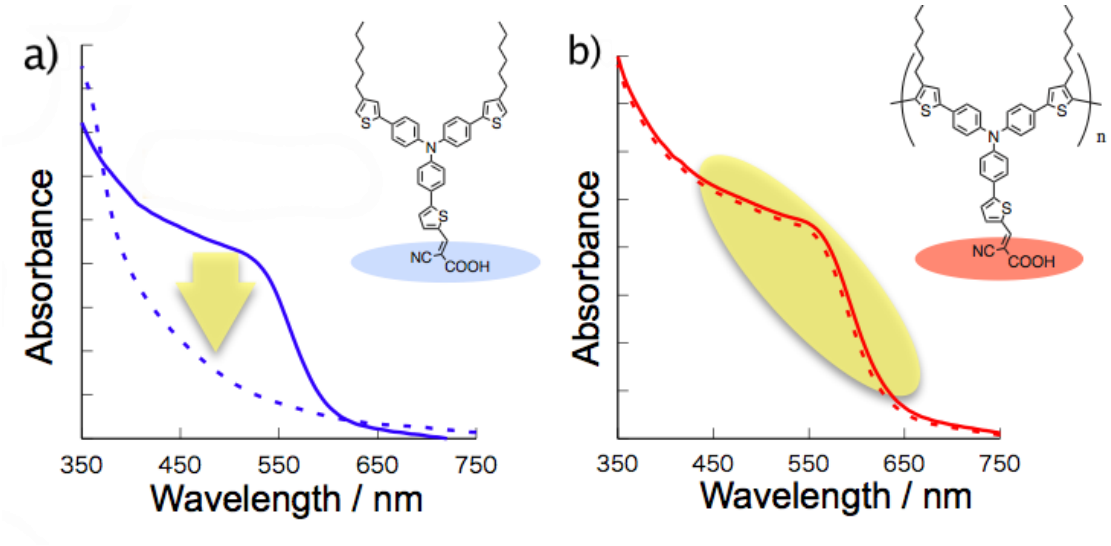


Figure 21: UV-Vis spectrum of the SA13 adsorbed $TiO_2$ a) before and b) after 100 cycles of cyclic voltammetry treatment. Dotted line shows the UV-Vis spectrum after immersing into methanol solution of 0.1M NaOH

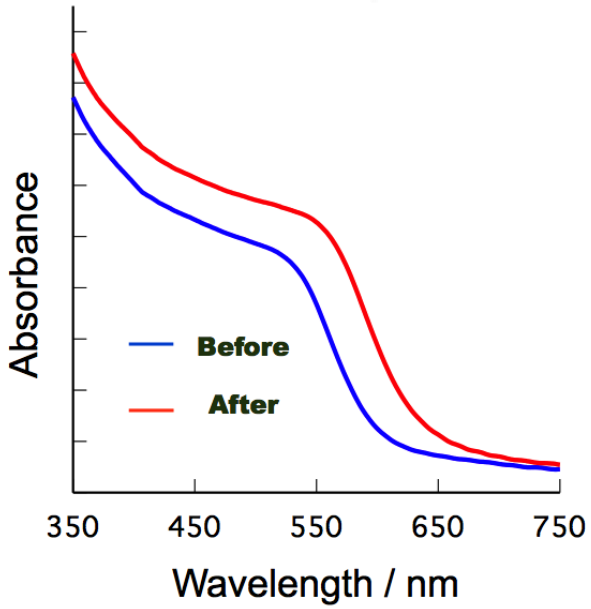


Figure 22: Absorption spectrum of SA13 adsorbed $TiO_2$ film, before and after 100 cycles of cyclic voltammetry treatment

Additionally, in order to evaluate the stability of polymeric dye on the adsorbed surface of the $TiO_2$ nanoparticles, the dye adsorbed $TiO_2$ electrode was first immersed into 0.1 M NaOH solution in methanol, then UV-Vis spectra was taken to observe the changes in conjugation length and the intensity of absorption with and without the cyclic treatment of +1.5 V potential.

As a result, the absorbance spectrum of the electrodes without the cyclic treatment showed quenching of the overall absorption (**Figure 21a)**, while those with the cyclic treatment showed preservation of both the spectrum pattern and intensity, which indicate that the cyclic treatment resulted in polymerization (**Figure 21b**). When the UV-Vis spectrum was taken on the dye-adsorbed $TiO_2$ electrode before and after the cyclic treatment of +1.5 V potential, the spectrum pattern exhibited a red shift and increased in the intensity of the absorption, indicating extension of conjugation length as well as a confirmation of dye polymerization (**Figure 22**).

## 4.3 Fabrication of EH-ECW

The working electrode of EH-ECW and platinum counter electrode for DSSC were fabricated through the method described by Ito et al. [53] The counter electrode with electrochromic film of PProDOT-$Me_2$ was deposited through electropolymerization using a chronoamperometry program. [4] Appendix C shows list of materials and the amount used for each processing step during the fabrication of EH-ECW.

### 4.3.1 Working electrode

The conductive glass substrate, FTO was purchased from Yamanaka glass (Japan), which of its thickness is 2.2 mm and sheet resistance of 6-8 Ω. FTO was first cleaned in aqueous detergent bath with ultrasonication for 10 minutes, then with double distilled water (18.2 Ω) for 10 minutes. They were rinsed with double distilled water and ethanol, then treated with UV-Ozone cleaner for 20 minutes. Titanium chloride ($TiCl_4$) treatment followed, where FTO was immersed in 40 mM $TiCl_4$ solution at 70 °C for 30 minutes. After rinsing with double distilled water and ethanol, it was treated with UV-Ozone cleaner again. $TiO_2$ paste (Dyesol 90T) was applied to FTO using a screen printing technique. The resulting $TiO_2$ layer has an area of 25 $mm^2$ (5 mm x

5 mm). The FTO with $TiO_2$ was sintered at 500 °C for 60 minutes with the ramp rate of 7 °C per minute.

The $TiO_2$ film on FTO (thereafter, working electrode) was treated with UV-Ozone cleaner for 20 minutes, then immersed in 26 mM $TiCl_4$ solution at 30 °C for 30 minutes. After rinsing with double distilled water and ethanol, working electrode was dried with Argon gas gun, heated to 500 °C and held there for 30 minutes on a hot plate, then cooled to 70 °C. Finally, working electrode was immersed into the dye solution for 18 hours in room temperature in dark.

### 4.3.2 Counter electrode substrate

In order to maximize the transparency of the overall cell at neutral state, the transmittance of different conductive glass was measured (**Figure 23**). While Yamanaka FTO exhibited the highest transmittance, ITO was chosen because of its suitability with electrochromism of PProDOT-$Me_2$.

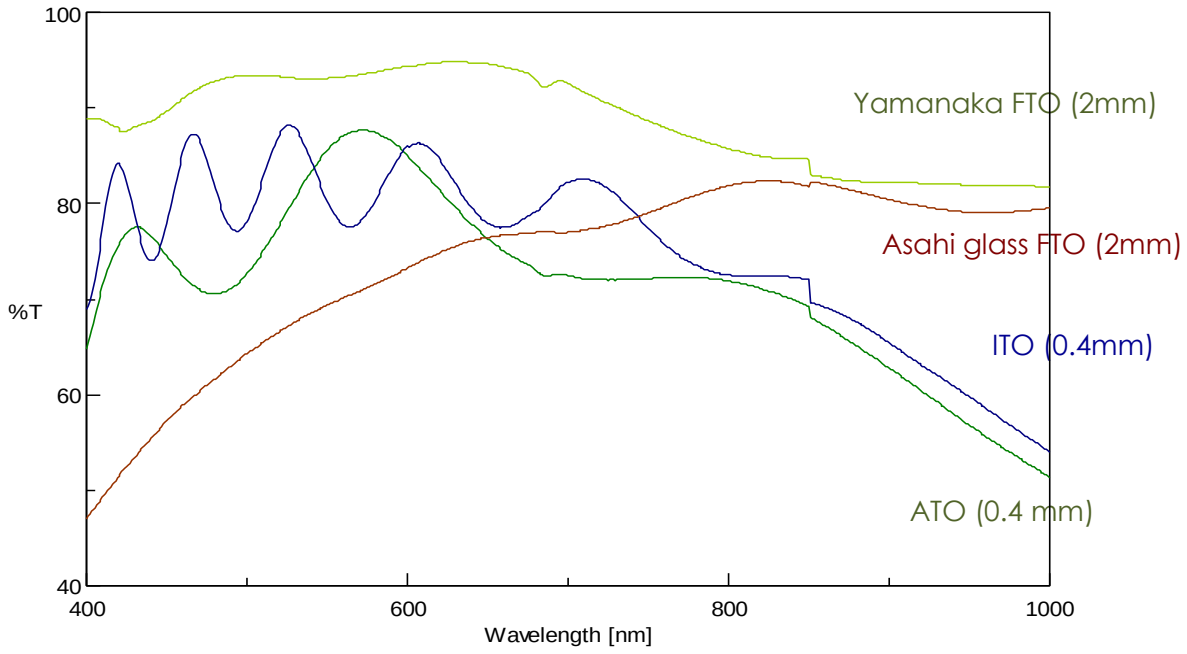


Figure 23: Transmittance of transparent conductive glasses

### 4.3.3 Platinum counter electrode

FTO was cut into desired dimension using diamond glass cutter and 2 holes were drilled using diamond tip drill bit. Then they were cleaned with double distilled water, acetone, and 0.1 M HCl for 5 minutes each twice. $H_2PtCl$ solution was applied, then they were heated to 450 °C for 30 minutes in air. The resulting counter electrode was cleaned with acetonitrile using a wipe, and it was heated to 450 °C for 30 minutes before use.

### 4.3.4 Counter electrode with organic materials (PProDOT-$Me_2$)

The cut and drilled ITO was cleaned in isopropyl alcohol for 10 minutes in ultrasonication. After drying by argon gas, ITO was placed in 90 °C oven for 30 minutes. 0.3 M ProDOT-$Me_2$ and 0.1 M $LiClO_4$ in acetonitrile was treated with argon gas replacement for 30 minutes. PProDOT-$Me_2$ film was deposited through electropolymerization technique using chronoamperometry program in Potentiostat (CH Instrument, Inc, Texas, U.S.). [4] The surface of the PProDOT-$Me_2$ deposited film was rinsed with ethanol before use.

### 4.3.5 Electrolyte

***Iodine electrolyte***

$I^-/I_3^-$ electrolyte was made through combining the materials and molarity shown in **Table 5.**

***Cobalt electrolyte***

The cobalt redox couple of $[Co(bpy)_3]^{2+/3+}$ was synthesized by method described by Feldt et al. [39] This particular couple of cobalt was chosen for the electrolyte for its desirable redox potential for the three sensitizers tested. The synthesis scheme is shown in Appendix B. The $[Co(bpy)_3]^{2+/3+}$ electrolyte solution was made through the following materials and molarity shown in **Table 5**.

Table 5: Electrolyte components

| Iodine | | Cobalt | |
|---|---|---|---|
| **Materials** | **Molarity [M]** | **Materials** | **Molarity [M]** |
| Iodine | 0.05 | $[Co(bpy)_3]^{2+}$ | 0.22 |
| Lithium Iodide | 0.1 | $[Co(bpy)_3]^{3+}$ | 0.02 |
| 1,2-dimethyl-3-propyl-imidazolium | 0.6 | $LiClO_4$ | 0.2 |
| Tert-butylpyridine | 0.5 | Tert-butylpyridine | 0.5 |
| Acetonitrile (solvent) | -- | Acetonitrile (solvent) | -- |

### 4.3.6 Device fabrication

Working electrode (WE) was rinsed with the solvent of dye solution. WE and counter electrode (CE) were assembled using heat curable adhesive called Surlyn (Dupont, U.S.) that cures at 120 °C. Electrolyte was injected through the holes between the electrodes using capillary action. The holes were sealed using Surlyn and a cover glass. Electrical contact was made through pasting colloidal silver liquid (Ted Pella, Inc CA, U.S.) to each electrode.

## 4.4 Characterization

### 4.4.1 Photovoltaic characterization

The photovoltaic performance of EH-ECW was characterized using OTENTO-SUN II Solar Simulator and SM-250 Hyper Mono Light System (Bunkokeiki Co., Tokyo, Japan) to measure I-V curve, and Incident to Photon Conversion Efficiency (IPCE), respectively. The mask (made of black paper) with an opening size of 0.25 $cm^2$ was used for all measurements.

### 4.4.2 Electrochromic characterization

For electrochromic property characterization, transmittance, cyclic amperometry, and charge capacitance measurements were conducted using UV-vis-IR spectrophotometer (V-570; JASCO, Tokyo, Japan). Often, Potentiostat (CH Instrument, Inc, Texas, U.S.) was used as a power source

in conjunction with UV-vis-IR spectrophotometer to measure the electrochromic properties during applied potential.

### 4.4.3 Durability testing

Durability of EH-ECW was evaluated through applying voltage between +1.5 V and 0 V, as well as -1.5 V and 0 V for 5 second each as one cycle using Potentiostat (CH Instrument, Inc, Texas, U.S.).

### 4.4.4 Electrochemical Impedance Spectroscopy

Electrochemical impedance of EH-ECW cells were evaluated through following the procedure by Adachi et al, between the frequency of 100 kHz-10 mHz and potential amplitude of 10 mV. PARSTAT 2263, Advanced Electrochemical System (Princeton Applied Research, Tennessee, U.S.) was utilized.

# Chapter 5: Results and Discussions

## 5.1 EH-ECW device design

In EH-ECW, the working electrode mounts transparent $TiO_2$ film (the average diameter of $TiO_2$: 30 nm, its thickness 5 μm) and organic dye (D35, SA8 or SA13), and cobalt (III/II) tris(2,2'-bipyridine) ($Co(bpy)^{+3/+2}$))was employed as electrolyte redox species **(Figure 24)**, for its kinetically fast charge transfer. [49] Organic EC polymer, PProDOT-$Me_2$ film serves as a counter electrode and an electrochromic layer of the EH-ECW device. The device functions as a photovoltaic cell upon illumination in short circuit, allowing external power storage. The stored energy can be used to perform electrochromism in the device by applying potential of +1.5 V on the working electrode, when the counter electrode is referenced as a ground, see Figure 23b. The potential difference drives the lithium cations to diffuse toward counter electrode, and induces electrochemical reduction of PProDOT-$Me_2$ layer. The EC layer becomes dark blue upon reduction, and remains transmissive light blue at DSSC state. During the colored state, there is no photocurrent generation from the dye molecules. The applied potential induces oxidation of working electrode, where the electrons in HOMO level of the dye become withdrawn toward $TiO_2$. The oxidized dye is quickly reduced by $Co^{+3}$ species to maintain equilibrium.

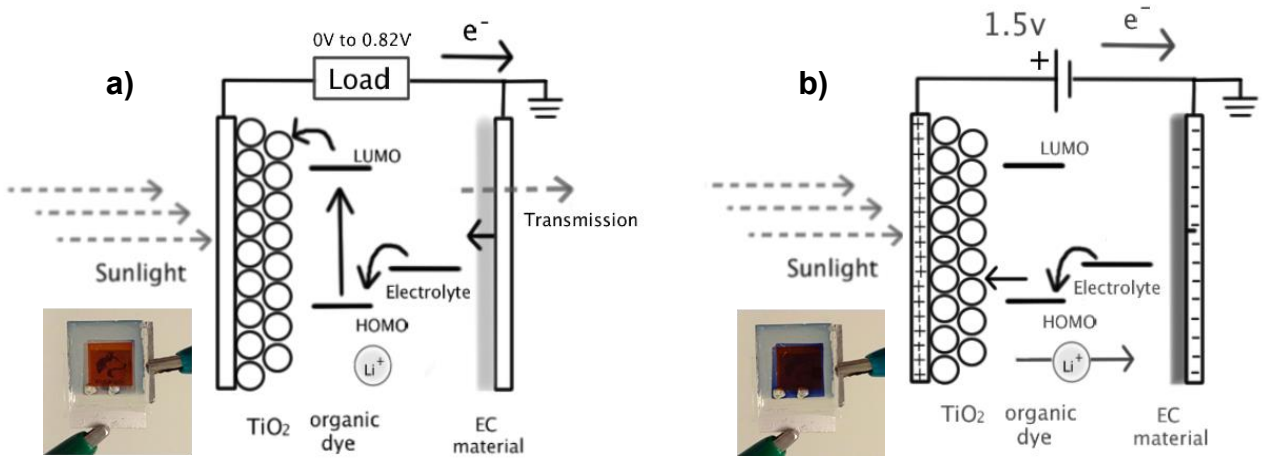


Figure 24: a) The neutral state (photovoltaic state) of EH-ECW where arrows indicate the flow of electrons, b) colored state of EH-ECW

The photovoltaic properties of EH-ECW with each of the 3 sensitizers (i.e. SA8, SA13, and D35) were analyzed and compared. The best photovoltaic performance was achieved by D35, but since it is unstable under cyclic potential, overall best performance is the DSSC with SA13, which demonstrated the PCE of 4.4 % ($V_{oc}$ = 0.82 V, $J_{sc}$ = 7.6 mA/cm$^2$, FF = 0.71) with the IPCE of 74 % **(Figure 25)**. Red shift was observed on the IPCE spectrum on Figure 25b from SA8 to SA13, which is consistent with SA13's narrower bandgap from Figure 13. The results imply that this dye possesses efficient electron injection due to its D-π-A structure. To assess the potential enhancement of durability through inclusion of polymeric site to the dye's molecular design, the photovoltaic properties of EH-ECW with various dye molecules were measured after 100 cycles of cyclic amperometry at +1.5 V. As a result, the photovoltaic properties of EH-ECW before and after the cyclic amperometry treatments were shown to have no major effect on the open circuit voltage ($V_{oc}$) or the short circuit current density ($J_{sc}$), but improvement of fill factor was observed for both SA8 and SA13 (**Table 6**). The increase in fill factor implies improved electron-transfer between the counter electrode and the redox species, where further

polymerization of EC polymer was induced by applied electric field. For D35, the overall performance was degraded after the cyclic treatment. The loss of $J_{sc}$ and $V_{oc}$ in D35's performance after the cyclic treatment suggests vulnerability of dye molecules without polymeric site against applied potential.

Table 6: Photovoltaic performance of EH-ECW with SA8, SA13, and D35

| Dye | Cyclic treatment | Voc [V] | Jsc [mA/cm2] | FF | PCE [%] |
|---|---|---|---|---|---|
| SA8 | Before | 0.78 | 6.5 | 0.68 | 3.5 |
| | After | 0.78 | 6.5 | 0.72 | 3.6 |
| SA13 | Before | 0.82 | 7.6 | 0.71 | 4.4 |
| | After | 0.82 | 7.5 | 0.74 | 4.5 |
| D35 | Before | 0.90 | 8.9 | 0.66 | 5.3 |
| | After | 0.84 | 8.6 | 0.69 | 5.0 |

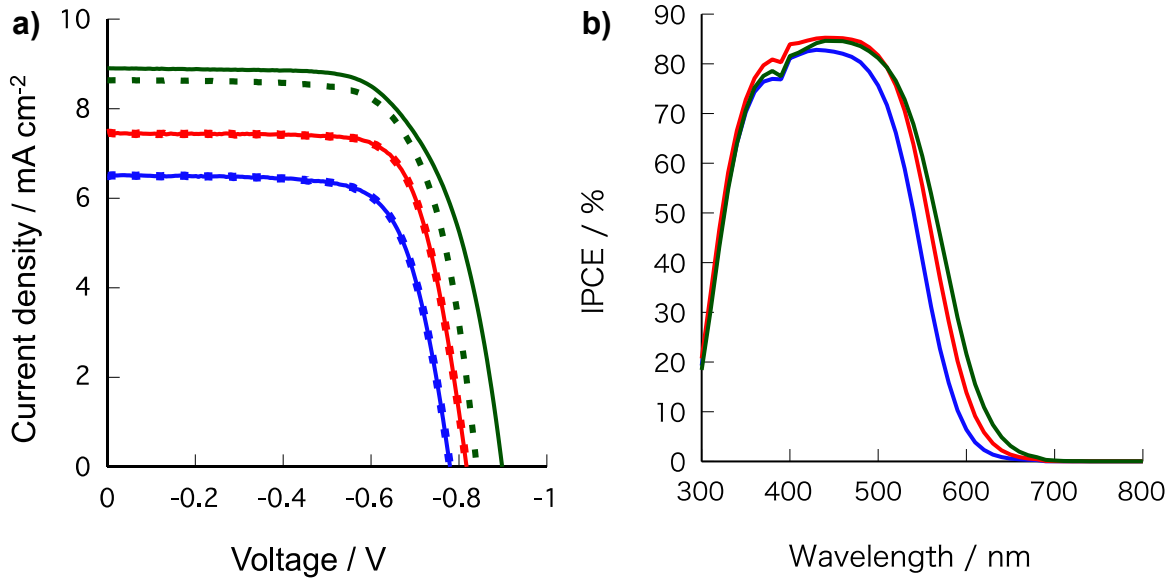


Figure 25: a) I-V curve of EH-ECW with SA8 (blue), SA13 (red), and D35 (green), before (solid line) and after (dotted line) 100 cycle of cyclic amperometry treatment b) IPCE curve of EH-ECW with the three dyes with the same color coding as I-V curve

The amount of adsorbed dye molecules on $TiO_2$ surface can be used as an indicator of the photovoltaic properties of EH-ECW. In another word, higher the amount of adsorbed dye, greater photocurrent generation is expected, but the transmittance may be lower since dye molecules are the major contributor of the absorption at visible range in the overall EH-ECW device. The dye adsorption amount was measured through immersing the dye adsorbed $TiO_2$ into 0.1 M NaOH solution; results for SA13 and D35 were $1.76 \times 10^{-5}$ mol $cm^{-3}$ and $1.79 \times 10^{-5}$ mol $cm^{-3}$, respectively. The close value of adsorbed amount for SA13 and D35 indicates that the functional property (i.e. photovoltaic property and transmittance) of SA13 does not depend on the adsorbed amount, but due to the structural difference.

## 5.2 Electrochromic properties

PProDOT-$Me_2$ is used as an effective cathodic coloring material (i.e. turns dark upon reduction) for polymer based ECW, [55] which exhibits high contrast ratio, rapid switching speed, and long-term cyclic stability when utilized in a device. [54] The polymer film of PProDOT-$Me_2$ forms a highly porous surface and exhibit good transmittance at neutral state. While the film transmittance depends on the electrolyte medium and counter ion storage layer, the ECW based on PProDOT-$Me_2$ as the working electrode material and $TiO_2/V_2O_5$ as the counter electrode material under applied modest potential of ±1.0 V~±1.5 V was found to result in good repeatability over 75,000 cycles. [4, 55] As shown in **Figure 26a**, between +1.5 V and 0 V, the maximum $\Delta T$ of 34 % (at 620 nm, $T_{max}$ = 43 %, $T_{min}$ = 9 %) was achieved for the EH-ECW with SA13 (**Figure 26 b**). Since the potential applied (1.5V) is larger than that of redox potential of SA13 (oxidation peak: 1.1 V, reduction peak: 0.5 V and 0.2 V (vs Ag/AgCl)) and EC polymer (oxidation peak: 0.13 V, reduction peak: 0.01 V (vs Ag/AgCl)), these organic molecules and the EC polymer undergo doping phenomena. The electrochromism of the sensitizer, SA13 upon +1.5

V on working electrode was evaluated through absorption spectrum measurement of SA13 adsorbed $TiO_2$ substrate. Upon applied potential of +1.5 V on the substrate in 0.1 M $LiClO_4$ in acetonitrile, $TiO_2$-SA13 is oxidized and showed increase in its absorbance, see **Figure 26c**. In the full device, applying +1.5 V drives the $TiO_2$-SA13 to oxidation, the counter electrode of PreDOT-Me2 becomes reduced stage, where both electrodess exhibit darker color. The switching speed of EH-ECW device of 0.25 $cm^2$ (5 mm x 5 mm) was determined to be 1 second evidenced in Figure 9 (b), owing to the fast redox process of PProDOT-$Me_2$ film.

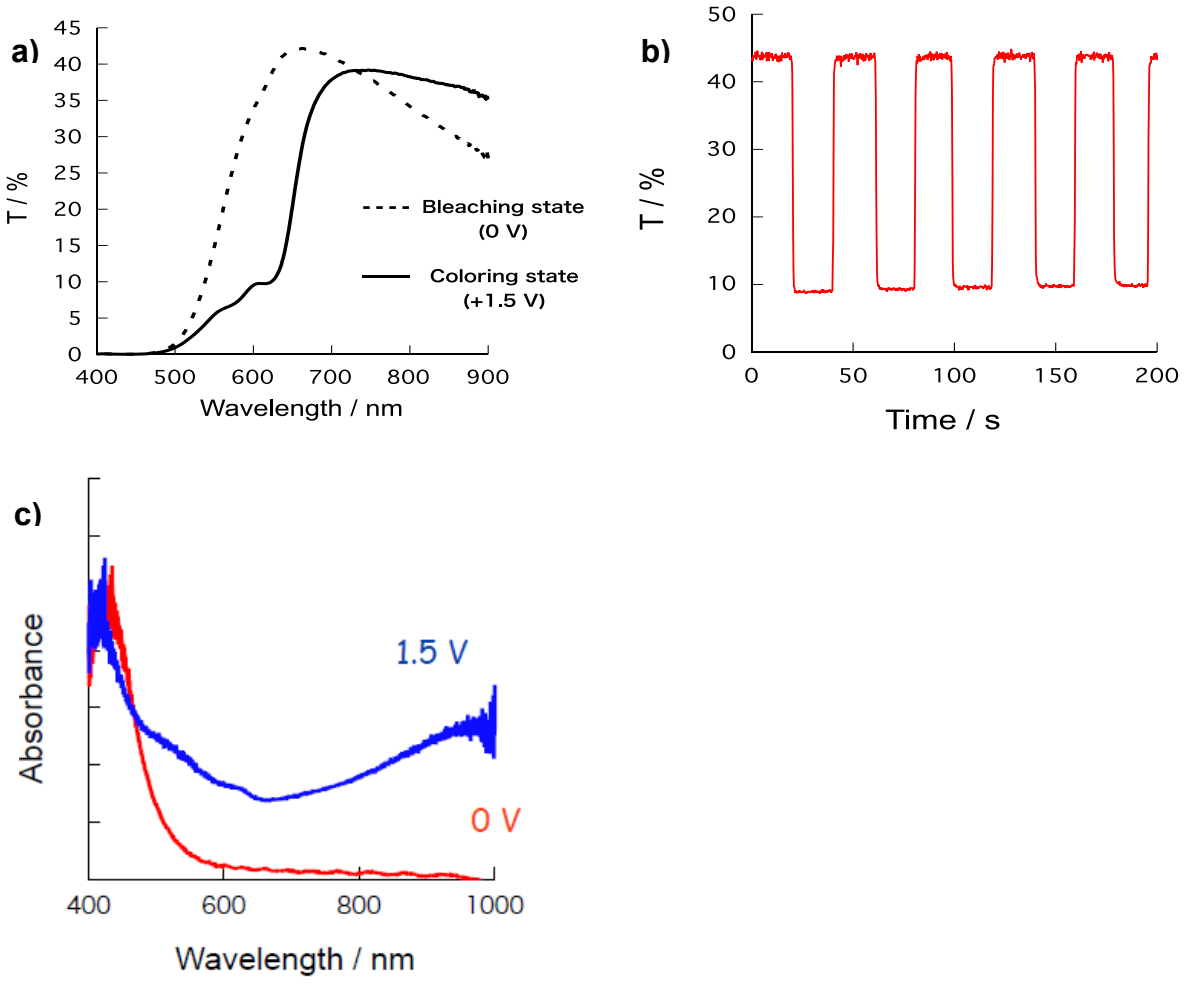


Figure 26: a) The transmittance spectrum between 400 nm and 900 nm of SA13 EH-ECW device, b) Time-course measurement of transmittance at 620 nm, and c) absorbance spectrum of SA13 mounted $TiO_2$ on FTO in 0.1 M $LiClO_4$ in acetonitrile solution at 0V (red) and at applied potential of 1.5 V (blue)

## 5.3 Cyclic stability

### 5.3.1 Electrochemical stability

Applying external potential to induce redox reactions of the electrochromic layer further drives the chemical stability of DSSC away from equilibrium. In order to assess the cyclic durability of EH-ECW, the devices of D35 and SA13 were subjected to +1.5 V to 0 V cyclic tests with the period of 10 seconds (5 seconds each step) for 5000 cycles. The results of cyclic current vs. time under constant voltage of +1.5 V over 100 cycles are shown in **Figure 27**, where the electrochemical stability of the EH-ECW with SA13 and the degradation with D35 are observed. As the number of cycles increases, the current flow of D35 mounted EH-ECW decreased; the D35 dye molecules were disturbed by the applied potential, which increased the internal interfacial resistance. On the other hand, the EH-ECW cell with SA13 exhibited constant stability benefitted from the polymeric structure. Upon repeatedly applied potential of + 1.5 V, SA13 dye molecules were polymerized, forming a polymer network, and became unsusceptible to electric field.

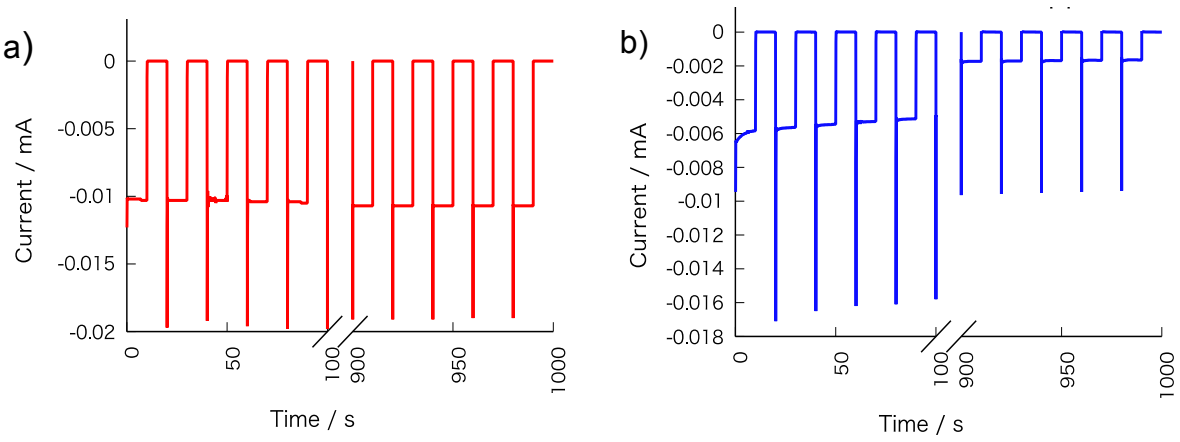


Figure 27: Chronocycleamperograms of SA13 a) and D35 b) applied +1.5 V on working electrode in 100 cycles with the period of 10 seconds

Electrochemical impedance spectroscopy (EIS) is a popular tool to observe the internal resistance of DSSC. EIS can also differentiate the impedance of one component from another, which makes it a very popular technique to evaluate the effectiveness of new material compared with conventional materials. In the EIS testing of EH-ECW, **Scheme 2** was utilized to analyze Nyquist plot. From Scheme 2, R1 corresponds to the ohmic resistance of the electrolyte and of the $TiO_2$. The parallel resistance capacitance (RC) circuits represent each electrochemical interface having a charge-transfer resistance in parallel with a nonideal double layer capacitance accounted for by a constant phase element. The short Warberg element accounts for the diffusional impedance (Nernst impedance) of the electrolyte in the cell. [49]

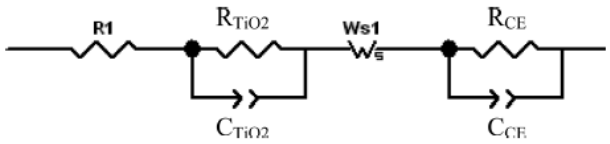


Scheme 2: Electrical equivalent circuit of the DSC under illumination at Voc [49]

EIS on EH-ECW was performed under illumination, and cyclic treatments were applied up to 8000 cycles, and the trend of Nyquist plot was observed. As shown in **Figure 28**, Ws1 (corresponds to the rightmost data point of the right semicircle) appears to be the most affected among all the components; it rapidly increased after 1000 cycles. Interestingly, no large difference between 1000 cycles and 2000 cycles were observed, but the increase was again obvious after 7000 cycles. The disturbance on $Co^{+3/+2}$ compounds in electrolytes appear to be not incremental. On the other hand, impedance of the counter electrode, $R_{PProDOT\text{-}Me2}$, also showed increase over cycles but not dramatically. These results suggest that loss of photovoltaic and electrochromic properties may be caused by the disturbance on $Co^{+3/+2}$ electrolyte.

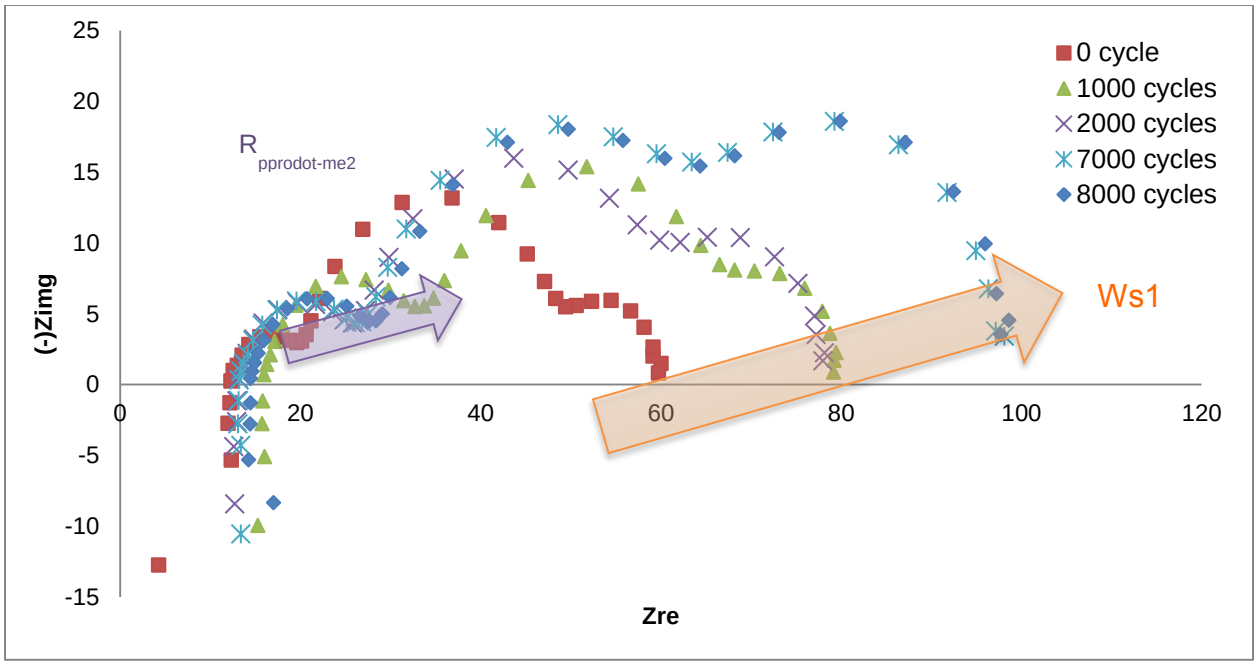


Figure 28: Electrochemical impedance measurement over cycles

### 5.3.2 Electrochromic stability

The stability of electrochromic properties were evaluated through measuring the transmittance spectrum after numerous cycles. The neutral state (**Figure 29**, **left**) showed about 7 % increase after 2000 cycles, and no major change was observed thereafter. Also, no shift in transmittance was observed, meaning no structural difference in the materials was induced through the cycles. On the other hand, transmittance at colored state displayed increase of transmittance over cycles (**Figure 29, right**), which indicates the loss of PProDOT-$Me_2$'s ability to become fully reduced.

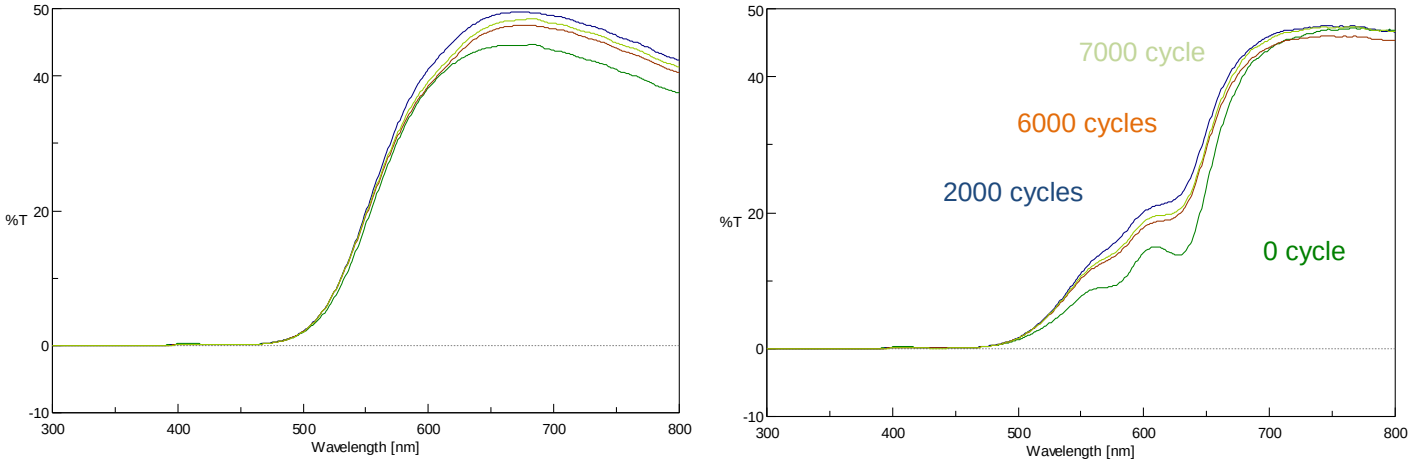


Figure 29: Transmittance spectrum of EH-ECW over cycles at neutral state (left) and reduced, colored state (right)

In order to observe the trend of % T over cycles, time course measurement of transmittance at the maximum ΔT (620 nm) was measured over 100 cycles. As **Figure 30a** shows, ΔT gradually decreased linearly up to about 600 seconds, then decreased logarithmically thereafter. This change is also observed from the current flow graph in **Figure 30b**, where the current flow began to decrease dramatically after around 600 seconds. Deterioration of PProDOT-$Me_2$ may have happened, but PProDOT-$Me_2$ has been proven to have good cyclic stability in device setting from previous researches. [4, 55] Other components, such as At the current stage of research, it is difficult to determine which component of EH-ECW is being deteriorated.

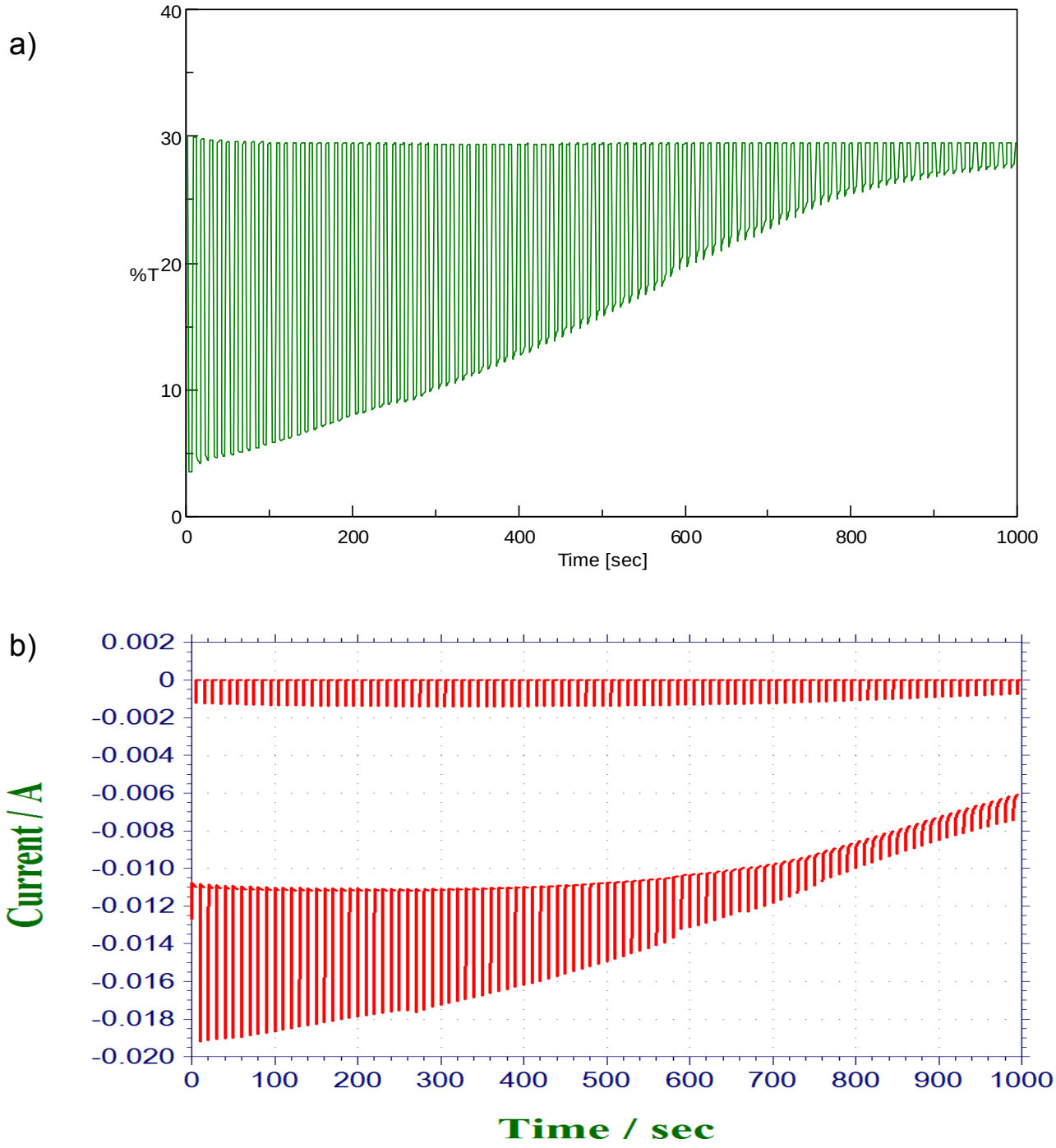


Figure 30: a) Time-course measurement and b) current flow of EH-ECW over 100 cycles

### 5.3.3 Photovoltaic stability

Furthermore, the photovoltaic properties of the EH-ECW with SA13 were evaluated at 100 cycles and at 5000 cycles. No major change in the overall efficiencies or the components of the

photovoltaic properties was observed and only 3 % degradation of PCE was observed after 5000 cycles, as shown in **Table 7**. Further investigation is needed to determine the effect of cyclic voltage on photovoltaic properties.

Table 7: Photovoltaic properties the EH-ECW with SA 13 after 5000 times of cyclic voltammogram

| Cycle | $V_{oc}$ [V] | $J_{sc}$ [mA $cm^{-1}$] | FF | PCE [%] |
|---|---|---|---|---|
| 0 | 0.85 | 6.5 | 0.69 | 3.8 |
| 100 | 0.87 | 6.4 | 0.70 | 3.9 |
| 5000 | 0.83 | 6.9 | 0.65 | 3.7 |

## 5.4 Power consumption

The energy balance of EH-ECW (i.e. power consumption vs. power generation) was computed from the device IV characteristics through sweeping the voltage between ±1.5 V on EH-ECW, as shown in **Figure 31**. Although photocurrent is generated under illumination, illumination does not improve the power dissipation during coloration. Photocurrent generation occurs under illumination, while EH-ECW consumes power under applied potential to become colored. The power consumption is shown in **Figure 32**, where the maximum power generated by EH-ECW (0.25 $cm^2$) was 1 mW, while dissipating 8 mW during colored state. Without the memory effect, constant voltage must be applied for the device to remain colored, and current EH-ECW design requires long period of time to generate sufficient power for electrochromism function.

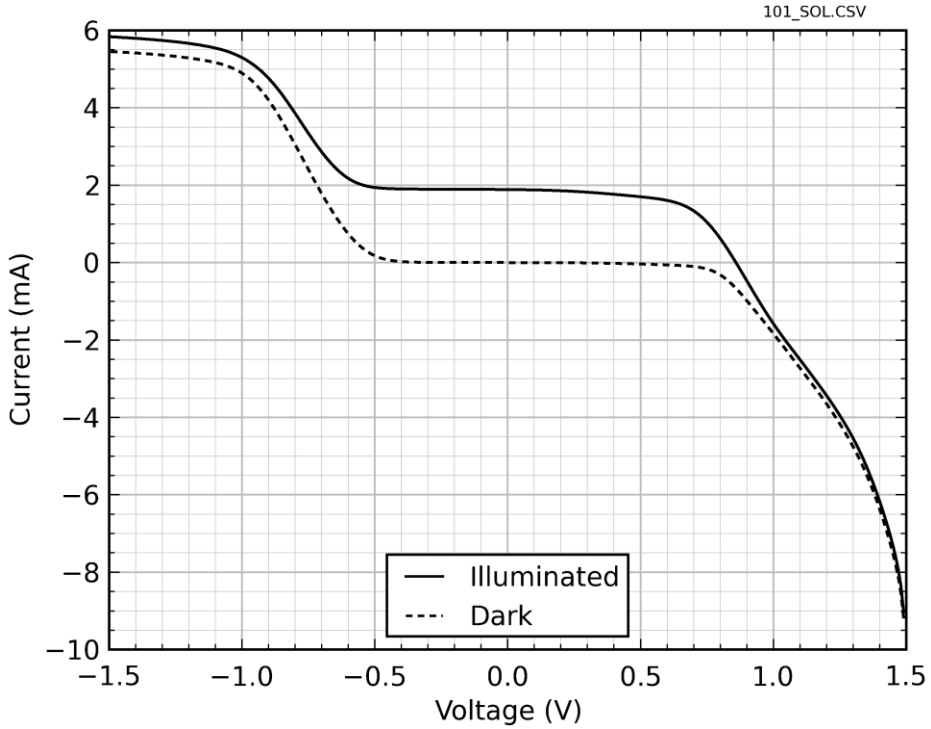


Figure 31: Measured current with different applied voltages, with and without illumination. The far left corresponds to the colorized state, while the far right corresponds to the bleached state. (Image courtesy of David Chamberlain).

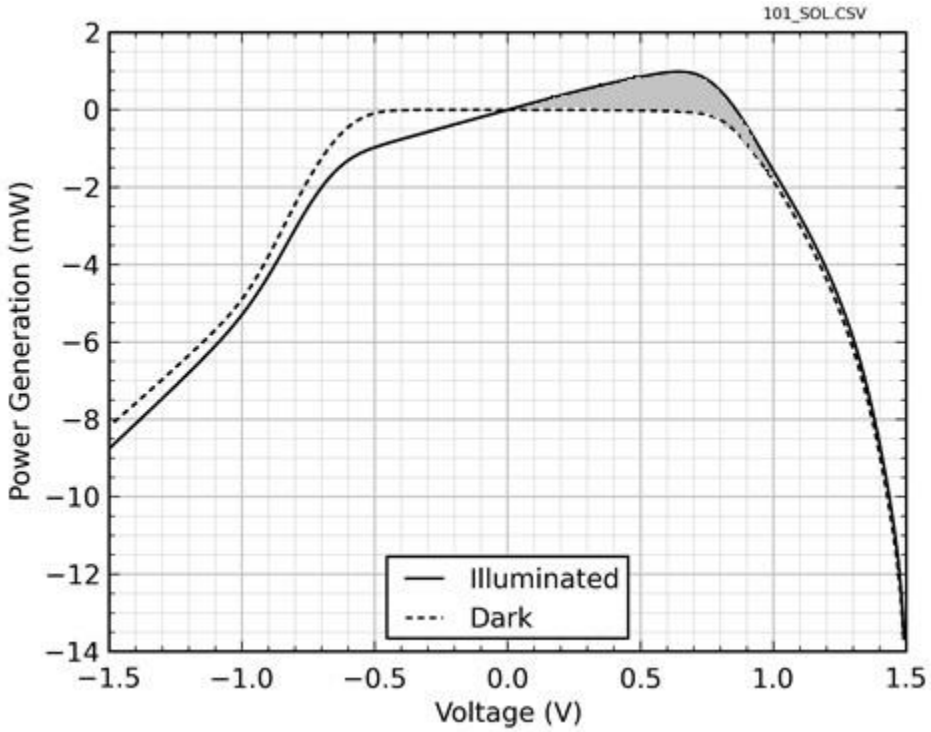


Figure 32: The power generated (or dissipated) by the EH-ECW with different voltages applied, with and without illumination. The far left corresponds to the colorized state, while the far right corresponds to the bleached state. Generated power is shown in the gray shading (Image courtesy of David Chamberlain).

# Chapter 6: Summary

## 6.1 Conclusions

In this study, we present a new design of self-powered electrochromic window called EH-ECW that exhibits tunable transmittance with $\Delta T = 34$ %, high photovoltaic performance of 4.5 %, and robust cyclic durability of both electrochromic and photovoltaic properties over 5000 cycles. The resulting device demonstrates fast switching rate of 1 second in both bleaching and coloring through the use of electrochromic polymer as a counter electrode layer for the cell area of 0.25 $cm^2$ (5 mm x 5 mm). In order to increase the transmittance of the device, cobalt redox couple and light colored organic dye were employed. In order to search for the best dye for the EH-ECW, we synthesized three different dye molecules, SA8, SA13 and D35, to find that the EH-ECW with SA13 exhibited the best performance. The organic dye of SA13 is not only an efficient sensitizer, but also contains durable polymeric structure, which contributed to high cyclic stability.

## 6.2 Recommendations

The ultimate goal of this study is to develop EH-ECW that has high photovoltaic properties (at least 4 % PCE), high electrochromic properties ($\Delta T$ = > 40 % within the visible spectrum at moderate voltage up to 1.5 V) and long term durability (>10,000 cycles). There are numerous recommendations for further analysis with the current design of EH-ECW as follows:

1. **Further electrochemical impedance spectroscopy analysis of current EH-ECW**

It is yet to be known the effect of applied potential on a device that possesses electrochemical and photovoltaic properties. Thus far, EIS was conducted to observe the relative changes in the overall cell. Ideally, changes in each component of the EH-ECW should be investigated, which

will lead to understanding which component should be altered. This assessment will also help understand the mechanism of EH-ECW.

**2. Development of transmissive dye**

Dye molecules are the major contributor of the low transmittance of EH-ECW at neutral state. In order to develop EH-ECW with high ΔT, transmittance at neutral (DSSC) state needs to be higher than the current design. However, dye molecules are innately colored to harvest energy from visible regions of solar spectrums. Transmissive dye may be developed through molecular engineering to absorb from IR and/or UV regions, although dye that absorbs sorely IR or UV region is unlikely to provide sufficient photocurrent for power generation. In order to provide sufficient photocurrent while retaining transmittance, tandem design of the device or co-sensitization of multiple dye molecules may be implemented. Another approach to increase the transmittance of EH-ECW is to develop an electrochromic dye that would turn transparent upon applied potential. Complementary electrochromic polymer should be mounted with this design.

**3. Alternative electrochromic polymer**

In this study, only one type of electrochromic polymer, PProDOT-$Me_2$ was tested for EH-ECW; however, most conductive polymers are electrochromic, which suggests that alternative electrochromic polymers may be explored for improved ΔT. Few suggestions include PEDOT and PProDOT-$Et_2$.

## Reference


1. Department of Energy, Buildings Sector, Building Energy Data Book, Buildingsdatabook.eren.doe.gov/ChapterIntro1.aspx (Retrieved September, 2013).

2. D. J. C. MacKay, *Sustainable Energy – Without the Hot Air*. UIT Cambridge, Cambridge, **2008**

3. C. G. Granqvist, E. Avendano, A. Azens, Thin Solid Films. **2003**, 442, 201.

4. S. Kim, M. Taya, C. Xu, *J. Electrochem. Soc*. **2009**, 160, 40.

5. Energy Films, Heat gain and heat loss through windows, http://www.energy-film.com/performance-data/ (Retrieved June, 2013).

6. R. Baetens, B. P. Jelle, A. Gustavsen, *Sol. Energy Mater. Sol. Cells.* **2010**, 94, 87.

7. P. R. Somani, S. Radhakrishnan, *Mater. Chem. Phys*. **2002**, 77, 117.

8. S. A. Jenekhe, *E 484/584 Course Pack*, University of Washington, Seattle, **2012.**

9. H. Shirakawa, E. J. Louis, A. G. Macdiarmid, C. K. Chiang, A. J. Heeger, *Chem. Comm*. **1977**, 478, 578.

10. R. E. Hummel, *Electronic Properties of Materials*. Springer-Verlag, Berlin, **1993**.

11. T. N. Kalyania, S. J. Dhoble, *Renew. Sust. Energ. Rev.* **2012**, 16, 5, 2696.

12. J. Zaumseil, H. Sirringhaus, *Chem. Rev.* **2007**, 107, 4, 1296.

13. G. A. H. Wetzelaer, M. Kuik, Y. Oliver, V. Lemaur, J. Cornil, S. Fabiano, M. A. Loi, P. W.M. Blom, *Phys. Rev. B.* **2012**, 86, 16, 165203.

14. P. M. Beanjuge, J. R. Reynolds, *Chem. Rev.* **2010**, 110, 1, 268.

15. G. A. Sotzing, J. L. Reddinger, A. R. Katritzky, J. Soloducho, R. Musgrave, J. R. Reynolds, P. J. Steel. *Chem. Mater*. **1997**, **9**, 1578.

16. H. Tsubomura, M. Matsumura, Y. Nomura, T. Amamiya, *Nature*, **1976**, 261, 402.

17. B. O'Regan, M. Gratzel, *Nature*, **1991**, 353, 737.

18. M. Grätzel, *J. Photochem. Photobiol. C.,* **2003**, 4, 145.

19. B. A. Gregg, *Endeavour.* **1997**, 21, 52.

20. M. Wang, C. Gratzel, S. M. Zakeeruddin, G. Michael. *Energy Environ. Sci.* **2012**, 5, 9394.

21. K. Kalyanasundaram, M. Graetzel, *Curr. Opin. Biotechnol.* **2010**, 21, 3, 298.

22. S. Zhang, X. Yang, Y. Numata, L. Han, *Energy Environ. Sci.* **2013**, 6, 1443.

23. M. Gratzel, *Accounts Chem. Res.* **2009**, 42, 11, 1788.

24. K. Hara, N. Koumura, *Material Matters: Alternative Energy Photovoltaics, Ionic Liquids, and MOFs*, **2009**, 4, 92.

25. C. Chou, M. Guo, K. Liu, Y. Chen, *Appl. Energ.* **2012**, 92, 224.

26. W. M. Campbell, A. K. Burrell, D. L. Officer, K. W. Jolley, *Coord. Chem. Rev.* **2004**, *248*, *9*, 817.

27. B. Oliva-Chatelain, A. Barron, An Introduction to Solar Cell Technology, http://cnx.org/content/m41217/1.1/ (Retrieved September, 2013)

28. N. Robertson, *Angew, Chem. Int. Ed. Engl.*, **2006**, 45, 2338.

29. M. K. Nazeeruddin, A. Kay, I. Rodicio, R. Humphry-Baker, E. Mueller, P. Liska, N. Vlachopoulos, M. Gratzel, *J. Am. Chem. Soc.*, **1993**, 115 , 14, 6382.

30. F. Gao, Y. Wang, D. Shi, J. Zhang, M. Wang, X. Jing, R. Humphry-Baker, P. Wang, S. M. Zakeeruddin, M. Gratzel, *J. Am. Chem. Soc.*,**2008**, 130, 32, 10720.

31. H. Nusbaumer, S. M. Zakeeruddin, J. E. Moser, M. Gratzel, *Chemistry: a European Journal*, **2003**, 9, 16, 3756.

32. Z. Huo, S. Dai, K. Wang, F. Kong, C. Zhang, X. Pan, X. Fang, *Sol. Energy Mater. Sol. Cells.* **2007**, 91, 20, 1959.

33. S. Colodrero, A. Mihi, L. Haggman, M. Ocana, G. Boschloo, A. Hagfeldt, H. Miquez. *Adv. Mater.*, **2009**, 21, 7, 764.

34. G. Rothenberger, P. Comte, M. Gratzel, *Sol. Energy Mater. Sol. Cells.* **1999**, 58, 321.

35. M. Wang, N. Chamberland, L. Breau, J-E. Moser, R. Humphry-Baker, B. Marsan, S. M. Zakeeruddin, M. Gratzel, *Nature Chemistry* **2010**, 2, 5, 385.

36. A. Yella, H-W. Lee, H. N. Tsao, C. Yi, A. K. Chandiran, M. K. Nazeeruddin, E. W-G. Diau, C-Y. Yeh, S. M. Zakeeruddin, M. Gratzel, *Science* **2011**, 334, 629.

37. B. A. Gregg, F. Pichot, S. Ferrere, C. L. Fields, *J. Phys. Chem. B* **2001**, 105, 1422.

38. S. K. Deb, S. Lee, C. E. Tracy, R. Pitts, B.A. Gregg, H. M. Branz, *Electrochem. Acta* **2001**, 46, 2125.

39. S. M. Feldt, E. A. Gibson, E. Gabrielsson, L. Sun, G. Boschloo, A. Hagfeldt, *J. Am. Chem. Soc.* **2010**, 132. 46, 16714.

40. C. Bechinger, J. N. Bullock, J. G. Zhang, E. E. Tracy, D. K. Benson, S. K. Deb, H. M. Branz, *J. Appl. Phys*. **1996**, 80, 1226.

41. K-S. Ahn, S. J. Yoo, M-S. Kang, J-W. Lee, Y-E. Sung, *J. Power Sources*. **2007**, 168, 2, 533.

42. U. Opara Krasovec, A. Georg, A. Georg, V. Wittwer, J. Luther, M. Topic, *Sol. Energy Mater. Sol. Cells*. **2004**, 84, 369.

43. C. Bechinger, S. Ferrere, A. Zaban, J. Sprague, B. A. Gregg, *Nature.* **1996**, 383, 608.

44. A. Hauch, A. Georg, S. Baumgartner, U. Opara Krasovec, B. Orel, *Electrochem. Acta* **2001**, 46, 2131.

45. C-Y. Hsu, K-M. Lee, J-H. Huang, K. R. Justin Thomas, J. T. Lin, K-H. Ho, *J. Power Sources*. **2008**, 185, doi:10.1016/j.jpowsour.2008.09.031.

46. S. Yang, J. Zheng, M. Li, C. Xu, *Sol. Energy Mater. Sol. Cells*. **2012**, 97, 186.

47. J. J. Wu, M. D. Hsieh, W. P. Liao, W. T. Wu, J. S. Chen, *ACS Nano.* **2009**, 3, 8, 2297.

48. H. Santa-Nokki, J. Kallioinen, J. Korppi-Tommola, *Photochem. Photobiol. Sci.* **2006**, 6, 63.

49. S. Carli, E. Busatto, S. Caramori, R. Boaretto, R. Argazzi, C. J. Timpson, C. A. Bignozzi, *J. Phys. Chem. C* **2013**, 117, 10.

50. H. N. Tsao, J. Burschka, C. Yi, F. Kessler, M. K. Nazeeruddin, M. Gratzel. *Energy Environ. Sci.* **2011**, 4, 12, 4921.

51. M. Kimura, R. Sakai, S. Sato, T. Fukawa, T. Ikehara, R. Maeda, T. Mihara, *Adv. Funct. Mater.* **2012**, 22, 469.

52. D. P. Hagberg, X. Jiang, E. Gabrielsson, M. Linder, T. Marinado, T. Brinck, A. Hagfeldt, L. Sun, *J. Mater. Chem*. **2009**, 19, 7232.

53. S. Ito, T. N. Murakami, P. Comte, P. Liska, C. Gratzel, M. K. Nazeeruddin, M. Gratzel, *Thin Solid Films* **2008**, 516, 4613.

54. A. Kumar, D. M. Welsh, M. C. Morvant, F. Piroux, K. A. Abboud, J. R. Reynolds, *Chem. Mater.* **1998**, 10, 896.

55. C. Xu, L. Lu, S. E. Leganski, D. Ning, M. Taya, *J. Mater. Res.* **2004**, 19, 7, 2072.

## Glossary

| | |
|---|---|
| %T | Percent Transmittance |
| ΔT | Transmittance difference (= $T_{max} - T_{min}$) |
| ATO | Antimony-doped Tin Oxide |
| CE | Counter electrode |
| $[Co(bpy)_3]^{3+/2+}$ | Cobalt (III/II) tris(2,2'- bipyridine) |
| DSSC | Dye-Sensitized Solar Cell |
| ECW | Electrochromic Window |
| EH-ECW | Energy-Harvesting Electrochromic Window |
| EIS | Electrochemical Impedance Spectroscopy |
| eV | Electron volt |
| FF | Fill factor |
| FTO | Fluorine-doped Tin Oxide |
| HOMO | Highest Occupied Molecular Orbital |
| $I^-/I_3^-$ | Iodine/Triiodine ions |
| IPCE | Incident monochromatic photon –to-electron conversion efficiency |
| ITO | Indium-doped Tin Oxide |
| I-V | Current to Voltage |
| $I_{sc}$ | Short-circuit current |

| | |
|---|---|
| $J_{sc}$ | Short-circuit current density |
| LUMO | Lowest Unoccupied Molecular Orbital |
| N3 | $RuL_2(NCS)_2$ complex, red dye |
| N719 | $RuL(NCS)_3$ complex, black dye |
| PEC | Photoelectrochromic |
| PCE | Power Conversion Efficiency |
| PEDOT | poly(3,4-ethylenedioxythiophene) |
| PProDOT | poly(3,4-propylenedioxythiophene) |
| PProDOT-$Me_2$ | poly (3,4-(2,2-dimethylpropylenedioxy)thiophene) |
| PProDOT-$Et_2$ | poly (3,4-(2,2-diethylpropylenedioxy)thiophene) |
| $TiO_2$ | Titanium Oxide |
| TPA | Triphenylamine |
| V | Voltage |
| $V_{oc}$ | Open-circuit voltage |
| WE | Working Electrode |

# Appendix

## A. Synthesis of SA13

*General*: $^1$HNMR spectra were measured on Bruker AVANCE 400 FT-NMR spectrometer. FT-IR spectra were obtained using a SHIMAZU FT-IR-8400 spectrometer.
*Materials*: All chemicals were purchased from commercial suppliers and used without purification. All solvents were distilled before each procedure. The purification of product was carried out by the combination of adsorption column chromatography (silica gel, Wakogel C-200) and recycling preparative HPLC (Japan Analytical Industry, Model LC-908). Analytical thin-layer chromatography was performed on commercial Merck plates coated with silica gel 60 $F_{254}$.
***Syntheses of SA-dyes:*** An oligothiophene monomer (SA8 and SA13) composed of central triphenyl amine, two peripheral thiophene and a carboxylic acid-substituted thiophene were synthesized by the four synthetic steps (**Scheme 1**).

*4-bromo-N-(4-bromophenyl)-N-[4-(2-thienyl)phenyl]-benzenamine* (1): Tris(4-bromophenyl)amine (0.53 g, $4.12\times10^{-3}$ mol) and 2-thiophenebronic acid (2.38 g, $4.95\times10^{-3}$ mol) were solved in THF (4 mL), toluene (3 mL) and 2.0M $K_2CO_3$ aqueous solution(2 mL). After degassing by nitrogen gas, t $Pd(PPh_3)_4$ (95 mg, $8.24\times10^{-4}$ mol) was added to the mixed solution. The reaction mixture was stirred at 75℃ for 48 h under nitrogen atmosphere. After 48 h, he reaction mixture was diluted with $CH_2Cl_2$ and washed with water. The organic layer was dried over $MgSO_4$ and concentrated under vacuum. The residue was purified by column chromatography on silica gel using $CH_2Cl_2$ as eluent to give **1** as white solid (0.80g, yield 40%). $^1$H-NMR($CDCl_3$, 400.13 MHz): δ=7.49 (d, *J*=8.80Hz, 2***H***, Ar***H***), 7.36 (d, *J*=6.40, 4***H***, Ar***H***), 7.24 (d, *J*=1.20Hz, 1***H***, Thiophene), 7.23 (m, 1***H***, Thiophene), 7.06 (m, 1***H***, Thiophene), 7.04 (d, *J*=8.80, 2***H***, Ar***H***), 6.96 (d, *J*=9.20, 4***H***, Ar*H*).

*5-[4-[bis(4-bromophenyl)amino]phenyl]-2-thiophenecarboxaldehyde* (2): To a cold solution of ***1*** (0.3 g, $6.18\times10^{-4}$ mol) in dry-DMF (1.5 mL) at 0℃ was added Vilsmeier reagent, which was prepared with $POCl_3$ (0.2 mL) in dry-DMF (0.5 mL). The mixture stirred at 70℃ for 4 h. After 4 h, the reaction mixture quenched 10% aqueous solution of NaOAc and extracted with $CH_2Cl_2$. The organic layer was dried over $MgSO_4$ and concentrated under vacuum. The residue was purified by column chromatography on silica gel using $CH_2Cl_2$ as eluent to give ***2*** as light-yellow solid (0.26 g, yield 81%). FT-IR (ATR); ν=1659 $cm^{-1}$ (-CHO). $^1$H-NMR ($CDCl_3$, 400.13 MHz): δ=9.87 (s, 1*H*, -C*H*O), 7.72 (d, *J*=3.60Hz, 1*H*, Thiophene), 7.54 (d, *J*=8.80, 2*H*, Ar*H*), 7.39 (d, *J*=9.60Hz, 4*H*, Ar*H*), 7.32 (d, *J*=3.60Hz, 1*H*, Thiophene), 7.06 (d, *J*=8.80Hz, 2*H*, Ar*H*), 6.99 (d, *J*=8.80, 4*H*, Ar*H*).

*5-[4-{bis(2-[3-hexylthiophene]phenyl)amino}phenyl]-2-thiophenecarboxaldehyde* (3): ***2*** (60 mg, $1.17\times10^{-4}$ mol) and 4-hexyl-2-(4,4,5,5-tetramethyl-1,3,2-dioxaborolan-2-yl)thiophene (86 mg, $2.92\times10^{-4}$ mol) were solved in THF (2 mL), toluene (1.5 mL) and 2.0M $K_2CO_3$ aqueous solution (1 mL). After degassing by nitrogen gas, $Pd(PPh_3)_4$ (5 mg, $4.68\times10^{-6}$ mol) was added to the mixed solution. The reaction mixture was stirred at 75℃ for 48 h under nitrogen atmosphere. After 48 h, the reaction mixture was diluted with $CH_2Cl_2$ and washed with water. The organic layer was dried over $MgSO_4$ and concentrated under vacuum. The residue was purified by column chromatography on silica gel using $CH_2Cl_2$ and hexane (ratio=1:1) as eluent to give ***4*** as orange oil (70 mg, yield 88%). $^1$H-NMR ($CDCl_3$, 400.13 MHz): δ=9.87 (s, 1***H***, -C***H*O**), 7.72 (d, *J*=3.60, 1*H*, Thiophene), 7.58 (d, *J*=8.80, 2***H***, Ar***H***), 7.37 (d, *J*=8.80, 4***H***, Ar***H***), 7.32 (d, *J*=3.60, 1***H***, Thiophene), 7.06 (m, 8***H***, Thiophene and Ar***H***), 6.98 (d, *J*=5.20, 4***H***, Ar***H***), 2.68 (t, *J*=8.00, 4***H***, -C$\boldsymbol{H_2}$-), 1.62 (m, 4***H***, -C$\boldsymbol{H_2}$-), 1.31 (m, 12***H***, -C$\boldsymbol{H_2}$-), 0.87 (t, *J*=6.80, 6***H***, -C$\boldsymbol{H_3}$).

*5-[4-{bis(2-[4-hexylthiophene]phenyl)amino}phenyl]-2-thiophenecarboxaldehyde* (4): ***2*** (0.1 g, $1.95\times10^{-4}$ mol) and 4-hexyl-2-(4,4,5,5-tetramethyl-1,3,2-dioxaborolan-2-yl)thiophene (0.14 g, $4.87\times10^{-4}$ mol) were solved in THF (4 mL), toluene (3 mL) and 2.0M $K_2CO_3$ aqueous solution (2 mL). After degassing by nitrogen gas, $Pd(PPh_3)_4$ (9 mg, $7.79\times10^{-6}$ mol) was added to the mixed solution. The reaction mixture was stirred at 75℃ for 48 h under nitrogen atmosphere. After 48 h, the reaction mixture was diluted with $CH_2Cl_2$ and washed with water. The organic layer was dried over $MgSO_4$ and concentrated under vacuum. The residue was purified by column chromatography on silica gel using $CH_2Cl_2$ and hexane (ratio=2:1) as eluent to give ***4*** as orange oil (47 mg, yield 36%). $^1$H-NMR ($CDCl_3$, 400.13 MHz): δ=9.86 (s, 1***H***, -C***H*O**), 7.71 (d, *J*=4.00, 1*H*, Thiophene), 7.55 (d, *J*=8.80, 2***H***, Ar***H***), 7.51 (d, 4***H***, Ar***H***), 7.32 (d, *J*=4.00, 1***H***, Thiophene), 7.12 (m, 6***H***, Ar***H***), 7.10 (s, 2***H***, Thiophene), 6.84 (s, 2***H***, Thiophene), 2.61 (t, *J*=4.40, 4***H***, -C$\boldsymbol{H_2}$-), 1.64 (m, 4***H***, -C$\boldsymbol{H_2}$-), 1.32 (m, 12***H***, -C$\boldsymbol{H_2}$-), 0.89 (t, *J*=6.80, 3***H***, -C$\boldsymbol{H_3}$).

*5-[4-{bis(2-[3-hexylthiophene]phenyl)amino}phenyl]-thienyl-2-cyanoacrylic acid = SA-8* : A solution of ***3*** (50 mg, $7.27\times10^{-5}$ mol) and cyanoacetic acid (9 mg, $1.09\times10^{-5}$ mol) in dry-acetonitrile (2 mL) and dry-toluene (1 mL) was refluxed at 90℃ in the presence of piperidine (0.13 mL) overnight. After cooling the mixture was diluted with $CH_2Cl_2$ and washed with 1.0M HCl aqueous and $H_2O$. The organic layer dried over $Na_2SO_4$ and concentrated under vacuum. The residue was purified by column chromatography on silica gel using $CH_2Cl_2$ and mixed solvent ($CH_2Cl_2$:MeOH = 9:1) in terms as eluent to give ***SA-8*** as dark-red solid (30mg, yield 55%). $^1$H-NMR ($CDCl_3$, 400.13 MHz): δ=8.32 (s, 1***H***, -C***H***-), 7.73 (d, *J*=3.60, 1*H*, Thiophene), 7.53 (d, *J*=8.80, 2***H***, Ar***H***), 7.35 (d, *J*=8.40, 4***H***, Ar***H***), 7.29 (d, *J*=3.60, 1***H***, Thiophene), 7.16 (m, 8***H***, Ar***H***), 6.96 (d, *J*=5.20, 2***H***, Thiophene), 2.66 (t, *J*=8.00, 4***H***, -C$\boldsymbol{H_2}$-), 1.61 (m, 4***H***, -C$\boldsymbol{H_2}$-), 1.29 (m, 12***H***, -C$\boldsymbol{H_2}$-), 0.86 (t, *J*=6.80, 6***H***, -C$\boldsymbol{H_3}$); $^{13}$C-NMR ($CDCl_3$, 100.61 MHz): δ=146.1, 146.0, 138.9, 137.7, 130.7, 130.0, 125.2, 123.8, 77.7, 77.4, 77.1, 32.0, 31.4, 29.6, 29.1, 23.0, 21.7, 14.5.

*5-[4-{bis(2-[4-hexylthiophene]phenyl)amino}phenyl]-thienyl-2-cyanoacrylic acid = SA-13* : A solution of ***4*** (40 mg, $5.81\times10^{-5}$ mol) and cyanoacetic acid (7 mg, $8.72\times10^{-5}$ mol) in dry-acetonitrile (2 mL) and dry-toluene (2 mL) was refluxed at 90℃ in the presence of piperidine (0.11 mL) overnight. After cooling the mixture was diluted with $CH_2Cl_2$ and washed with 1.0M HCl aqueous and $H_2O$. The organic layer dried over $Na_2SO_4$ and concentrated under vacuum. The residue was purified by column chromatography on silica gel using $CH_2Cl_2$ and mixed solvent ($CH_2Cl_2$:MeOH = 9:1) in terms as eluent to give ***SA-13*** as dark-red solid (40mg, yield 91%). $^1$H-NMR ($CDCl_3$, 400.13 MHz): δ=8.32 (s, 1***H***, -C***H***-), 7.75 (m, 1*H*, Thiophene), 7.49 (m, 6***H***, Ar***H***), 7.29 (m, 1***H***, Thiophene), 7.09 (m, 8***H***, Ar***H*** and Thiophene), 6.83 (s, 2***H***, Thiophene), 2.59 (t, *J*=7.20, 4***H***, -C$\boldsymbol{H_2}$-), 1.65 (m, 4***H***, -C$\boldsymbol{H_2}$-), 1.32 (m, 12***H***, -C$\boldsymbol{H_2}$-), 0.88 (m, 3***H***, -C$\boldsymbol{H_3}$); $^{13}$C-NMR ($CDCl_3$, 100.61 MHz): δ=145.6, 144.4, 143.3, 126.8, 125.2, 124.2, 122.6, 119.2, 77.4, 77.0, 76.7, 31.7, 30.7, 30.4, 29.0, 22.7, 14.1.

## B. Synthetic route of $[Co(bpy)_3]^{3+/2+}$

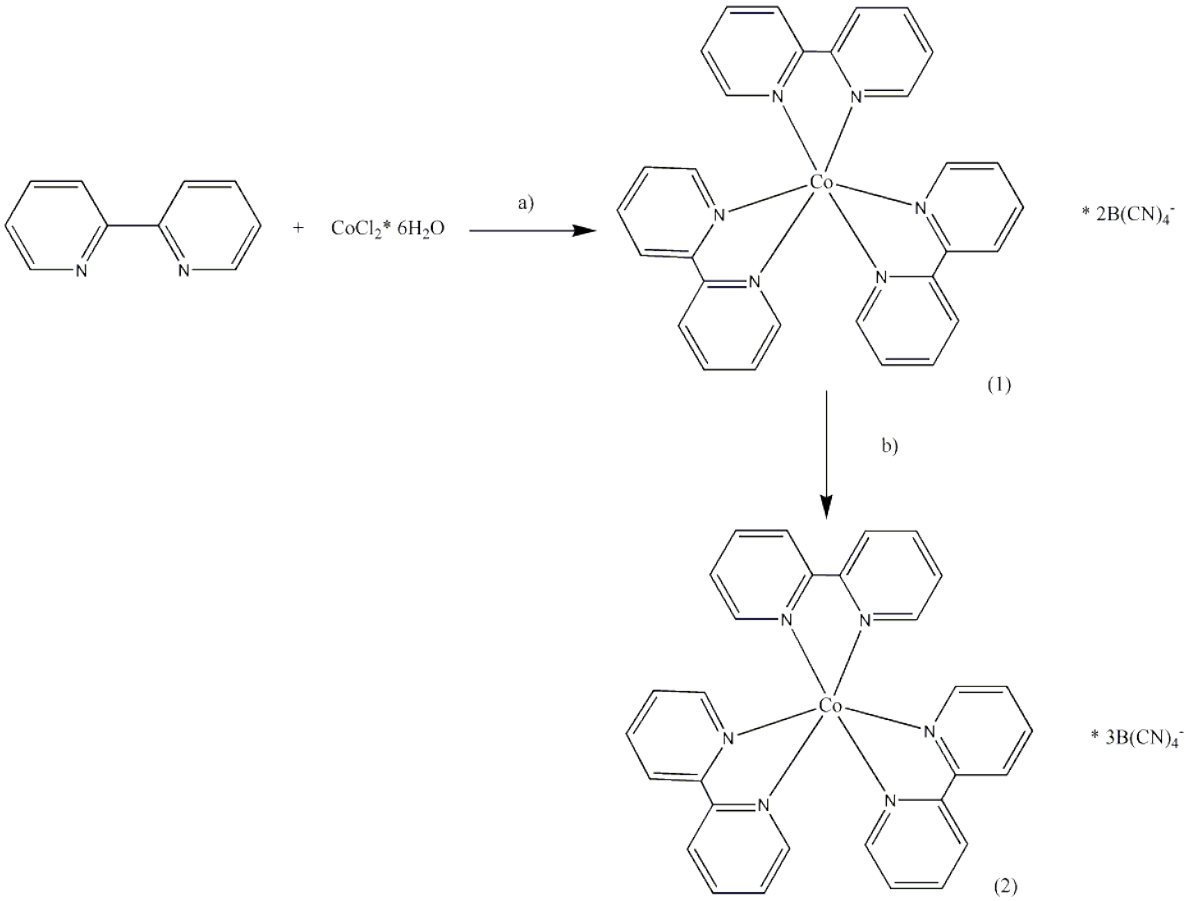


Figure 33: Synthesis scheme of (1) $[Co(bpy)_3]^{2+}$ and (2) $[Co(bpy)_3]^{3+}$. Reagents and conditions: a) $Kb(CN)_4$ and methanol, 2 hr at room temperature and b) $NOBF_4$, $KB(CN)_4$ and methanol at room temperature.

## C. List of materials used for the fabrication of EH-ECW

| Material component | Name | Function/Purpose | Per process | Number of DSSCs[1] | 1 DSSC | unit |
|---|---|---|---|---|---|---|
| Working electrode | FTO glass | electrode substrate | 12.25 | 4 | 3.0625 | $cm^2$ |
| | $TiO_2$ paste | working electrode | 3 | 16 | 0.1875 | g |
| | Toluene | dye solvent | 62.7 | 58[2] | 1.081034 | mg |
| | Dye (SA13) | Dye | 14.2 | 58 | 0.244828 | mg |
| | $TiCl_4$ solution | passivation layer treatment on FTO | 2 | 16 | 0.125 | mL |
| | $H_2O$ | passivation layer treatment on FTO | 48 | 16 | 3 | mL |
| | $TiCl_4$ solution | passivation layer treatment on $TiO_2$ | 250 | 6 | 41.66667 | µL |
| | $H_2O$ | passivation layer treatment on $TiO_2$ | 50 | 6 | 8.333333 | mL |
| Counter electrode | ITO glass | electrode substrate | 3 | 1 | 3 | $cm^2$ |
| | ProDOT-$Me_2$ | Counter electrode | 0.15 | 10 | 0.015 | g |
| | Acetonitrile | solvent for electropolymerization | 50 | 10 | 5 | mL |
| | $LiClO_4$ | electrolyte component for electropolymerization | 0.532 | 10 | 0.0532 | g |
| Electrlyte | $[Co(bpy)_3]^{2+}$ | Redox couple--oxidizing agent | 49.98 | 20 | 2.499 | mg |
| | $[Co(bpy)_3]^{3+}$ | Redox couple--reducing agent | 5.23 | 20 | 0.2615 | mg |
| | $LiClO_4$ | ion | 6.38 | 20 | 0.319 | mg |
| | Tert-butylpyridine | ion | 20.28 | 20 | 1.014 | mg |
| | Acetonitrile | solvent | 0.3 | 20 | 0.015 | mL |
| | Electrolyte | Electrolyte insertion | 0.0051 | 1 | 0.0051 | g |
| Assembly | Surlyn tape | adhesive | 2.25 | 1 | 2.25 | cm2 |
| | Cover glass | Sealant | 0.7 | 1 | 0.7 | cm2 |

1. Number of DSSCs refers to the number of DSSCs that are usually made through a process.
2. The number of DSSCs made were computed using the value from amount of adsorbed dye [$M/cm^3$] and its molarity in the dye solution [M/L].